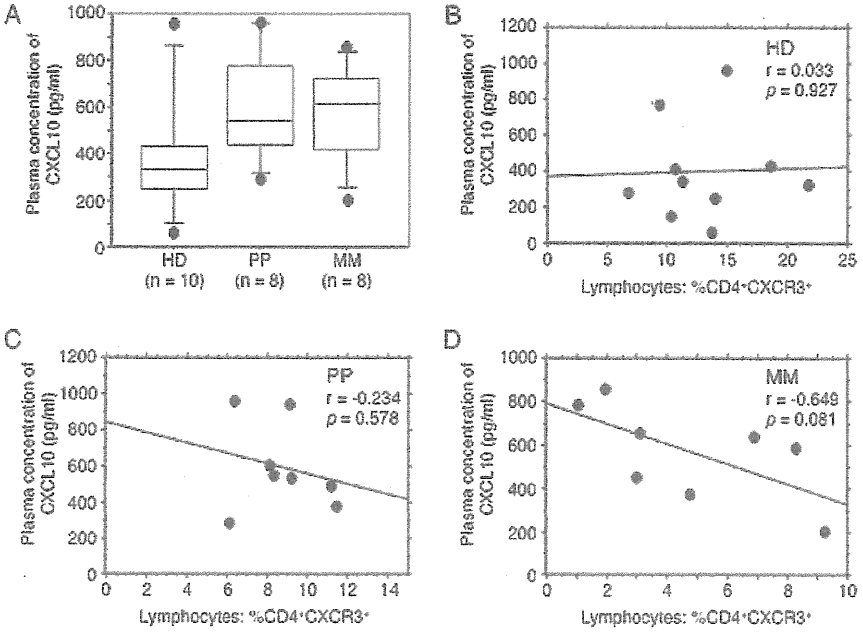

Figure 7. Modest inverse correlation between the population size of $CD4^+CXCR3^+$ T cells and plasma CXCL10 levels in MMs. (*A*) Plasma concentration of CXCL10/IP10 from HDs (n = 10), PPs (n = 8), and MMs (n = 8). The box plot is presented as described in Figure 3. Correlations between the percentage of $CD4^+CXCR3^+$ T cells in gated lymphocytes and plasma concentration of CXCL10/IP10 from HDs (*B*), PPs (C), and MMs (*D*) were analyzed using Spearman's rank correlation test.

duction. These results suggest that $CD4^+$ T cells from MMs already possess a reduced capacity to produce IFN-γ, which is important for activation of antitumor immune function due to long-term asbestos exposure and the presence of tumor. A correlation test showed that mRNA levels of IFN-γ in PPs tended to increase in stimulated $CD4^+$ T cells with decreasing surface CXCR3 expression levels, although mRNA levels of IFN-γ in HDs were positively correlated with CXCR3 expression. Given that asbestos exposure is partially associated with autoimmune responses (43), asbestos exposure in PPs might change the character of $CD4^+$ T cells to enhance antitumor immune function, and IFN-γ mRNA expression might not be suppressed in patients with PP who do not have MM.

Alternatively, the producible capacities of IL-6 in stimulated $CD4^+$ T cells tended to be higher in PPs and MMs compared with HDs, suggesting that asbestos exposure enhances inflammatory cytokine producibility in $CD4^+$ T cells. We showed previously that the plasma concentration of IL-6 in MM was higher than that of HDs and PPs (44). Given that the levels of plasma IL-6 were not high in PPs, it seems that plasma IL-6 in MMs is mainly derived from mesothelioma cells (45–47). Furthermore, IL-6 inhibits Th1-cell differentiation and promotes Th2-cell differentiation (48). Thus, plasma IL-6 might induce decreased IFN-γ mRNA expression and increased IL-4 production in stimulated $CD4^+$ T cells from MMs. On the other hand, although there were no significant differences in IL-10 and IL-17A production under these experimental conditions, there are several reports regarding the relationship between IL-10/IL-17 and cancer status, which indicates that IL-10 may suppress antitumor immune function and that IL-17 may promote inflammation in cancer (49, 50). Future studies should therefore investigate the pathophysiological roles of IL-10 and IL-17 in asbestos-exposed patients such as those with PPs or MMs.

Finally, we found that the plasma concentration of CXCL10/IP10 tended to be higher for PPs and MMs than HDs. Furthermore, there tended to be an inverse correlation between the population of $CD4^+CXCR3^+$ T cells in lymphocytes and the plasma concentration of CXCL10/IP10 in MMs but not in HDs or PPs. These results indicated that antitumor immune function in MMs may be impaired after reduction of $CD4^+CXCR3^+$ T cells in lymphocytes because CXCL10/IP10 from monocytes, endothelial cells, fibroblasts, mesothelial cells, and mesothelioma in the region of existing tethered asbestos and a cancerous lesion attracts antiinflammatory or antitumor T cells.

In conclusion, this study revealed that reduction of CXCR3 expression in human peripheral $CD4^+$ T cells occurred after chronic exposure to chrysotile. This finding suggests that antitumor immunity might not function normally in patients with asbestos-related disease because the low expression of CXCR3 induces depressed chemotaxis. Additionally, it seems that IFN-γ expression is inhibited by the occurrence of mesothelioma rather than asbestos exposure, and the weak production of IFN-γ leads to suppression of antitumor activity. Further research of chemokine-mediated migration dependent on CXCR3 expression is required to determine the mechanism of immune dysfunction via chemokine receptors after exposure to asbestos and to investigate the use of the chemokine receptor CXCR3 as a key molecule in immunotherapy strategies for asbestos-related disease. In addition, these molecules may be effective tools for the detection of asbestos exposure, considering our previous findings of enhanced Bcl-2 expression in $CD4^+$ T cells from MMs (16) and higher plasma concentration of IL-6, IL-10, and TGF-β (44). For example, higher plasma IL-10 and TGF-β with lower INF-γ expression may be interpreted as an enhanced regulatory T-cell activity overcoming antitumor T-cell activity in MMs.

Further studies regarding the size and function of regulatory T cells in MMs and the *in vitro* model using the cell line should be performed to better understand immunological status among asbestos-exposed patients with or without mesothelioma. Moreover, a device to evaluate total antitumor activities in these patients using the degree of reduced expression in $CD4^+$ T cells of an NK cell–activating surface receptor such as NKp46, including CXCR3 and IFN-γ expression, may assist in the diagnosis of MMs and reveal good prognostic factors for these patients.

Author Disclosure: None of the authors has a financial relationship with a commercial entity that has an interest in the subject of this manuscript.

Acknowledgments: The authors thank Ms. Tamayo Hatayama, Minako Kato, Naomi Miyahara, Shoko Yamamoto, Misao Kuroki, Keiko Kimura, Yoshiko Yamashita, and Tomoko Sueishi for technical help.

References

1. Upadhyay D, Kamp DW. Asbestos-induced pulmonary toxicity: role of DNA damage and apoptosis. *Exp Biol Med (Maywood)* 2003;228: 650–659.
2. Panduri V, Surapureddi S, Soberanes S, Weitzman SA, Chandel N, Kamp DW. P53 mediates amosite asbestos-induced alveolar epithelial cell mitochondria-regulated apoptosis. *Am J Respir Cell Mol Biol* 2006;34:443–452.
3. Upadhyay D, Panduri V, Kamp DW. Fibroblast growth factor-10 prevents asbestos-induced alveolar epithelial cell apoptosis by a mitogen-activated protein kinase-dependent mechanism. *Am J Respir Cell Mol Biol* 2005; 32:232–238.
4. Mossman BT. Introduction to serial reviews on the role of reactive oxygen and nitrogen species (ROS/RNS) in lung injury and diseases. *Free Radic Biol Med* 2003;34:1115–1116.
5. Kamp DW, Panduri V, Weitzman SA, Chandel N. Asbestos-induced alveolar epithelial cell apoptosis: role of mitochondrial dysfunction caused by iron-derived free radicals. *Mol Cell Biochem* 2002;234–235: 153–160.
6. Jiang L, Nagai H, Ohara H, Hara S, Tachibana M, Hirano S, Shinohara Y, Kohyama N, Akatsuka S, Toyokuni S. Characteristics and modifying factors of asbestos-induced oxidative DNA damage. *Cancer Sci* 2008; 99:2142–2151.
7. Petrilli V, Dostert C, Muruve DA, Tschopp J. The inflammasome: a danger sensing complex triggering innate immunity. *Curr Opin Immunol* 2007; 19:615–622.
8. Sutterwala FS, Ogura Y, Flavell RA. The inflammasome in pathogen recognition and inflammation. *J Leukoc Biol* 2007;82:259–264.
9. Cook GP, Savic S, Wittmann M, McDermott MF. The NLRP3 inflammasome, a target for therapy in diverse disease states. *Eur J Immunol* 2010;40:631–634.
10. Kannerstein M, Churg J, McCaughey E, Selikoff IJ. Pathogenic effects of asbestos. *Arch Pathol Lab Med* 1977;101:623–628.
11. Kannerstein M, Churg J, McCaughey WT. Asbestos and mesothelioma: a review. *Pathol Annu* 1978;13:81–129.
12. Craighead JE, Mossman BT. The pathogenesis of asbestos-associated diseases. *N Engl J Med* 1982;306:1446–1455.
13. Miyoshi I, Kubonishi I, Yoshimoto S, Shiraishi Y. A T-cell line derived from normal human cord leukocytes by co-culturing with human leukemic T-cells. *Gann* 1981;72:978–981.
14. Miyoshi I, Kubonishi I, Yoshimoto S, Akagi T, Ohtsuki Y, Shiraishi Y, Nagata K, Hinuma Y. Type c virus particles in a cord T-cell line derived by co-cultivating normal human cord leukocytes and human leukaemic T cells. *Nature* 1981;294:770–771.
15. Hyodoh F, Takata-Tomokuni A, Miura Y, Sakaguchi H, Hatayama T, Hatada S, Katsuyama H, Matsuo Y, Otsuki T. Inhibitory effects of anti-oxidants on apoptosis of a human polyclonal T-cell line, MT-2, induced by an asbestos, chrysotile-A. *Scand J Immunol* 2005;61:442–448.
16. Miura Y, Nishimura Y, Katsuyama H, Maeda M, Hayashi H, Dong M, Hyodoh F, Tomita M, Matsuo Y, Uesaka A, *et al.* Involvement of IL-10 and Bcl-2 in resistance against an asbestos-induced apoptosis of T cells. *Apoptosis* 2006;11:1825–1835.
17. Otsuki T, Miura Y, Nishimura Y, Hyodoh F, Takata A, Kusaka M, Katsuyama H, Tomita M, Ueki A, Kishimoto T. Alterations of Fas and Fas-related molecules in patients with silicosis. *Exp Biol Med (Maywood)* 2006;231:522–533.
18. Otsuki T, Maeda M, Murakami S, Hayashi H, Miura Y, Kusaka M, Nakano T, Fukuoka K, Kishimoto T, Hyodoh F, *et al.* Immunological effects of silica and asbestos. *Cell Mol Immunol* 2007;4:261–268.
19. Maeda M, Nishimura Y, Hayashi H, Kumagai N, Chen Y, Murakami S, Miura Y, Hiratsuka JI, Kishimoto T, Otsuki T. Reduction of CXCR3 in an *in vitro* model of continuous asbestos exposure on a human T-cell line, MT-2. *Am J Respir Cell Mol Biol* (In press)
20. Homey B, Muller A, Zlotnik A. Chemokines: agents for the immunotherapy of cancer? *Nat Rev Immunol* 2002;2:175–184.
21. Rudge G, Barrett SP, Scott B, van Driel IR. Infiltration of a mesothelioma by IFN-gamma-producing cells and tumor rejection after depletion of regulatory T cells. *J Immunol* 2007;178:4089–4096.
22. Miller CH, Maher SG, Young HA. Clinical use of interferon-gamma. *Ann N Y Acad Sci* 2009;1182:69–79.
23. Rockley PF, Tyring SK. Interferons alpha, beta and gamma therapy of anogenital human papillomavirus infections. *Pharmacol Ther* 1995;65: 265–287.
24. Welsh RM, Lin MY, Lohman BL, Varga SM, Zarozinski CC, Selin LK. Alpha beta and gamma delta T-cell networks and their roles in natural resistance to viral infections. *Immunol Rev* 1997;159: 79–93.
25. Pan J, Burdick MD, Belperio JA, Xue YY, Gerard C, Sharma S, Dubinett SM, Strieter RM. CXCR3/CXCR3 ligand biological axis impairs RENCA tumor growth by a mechanism of immunoangiostasis. *J Immunol* 2006;176:1456–1464.
26. Liu Y, Poon RT, Feng X, Yu WC, Luk JM, Fan ST. Reduced expression of chemokine receptors on peripheral blood lymphocytes in patients with hepatocellular carcinoma. *Am J Gastroenterol* 2004;99:1111–1121.
27. Liu Y, Poon RT, Hughes J, Feng X, Yu WC, Fan ST. Chemokine receptors support infiltration of lymphocyte subpopulations in human hepatocellular carcinoma. *Clin Immunol* 2005;114:174–182.
28. Winter D, Moser J, Kriehuber E, Wiesner C, Knobler R, Trautinger F, Bombosi P, Stingl G, Petzelbauer P, Rot A, *et al.* Down-modulation of CXCR3 surface expression and function in CD8+ T cells from cutaneous T cell lymphoma patients. *J Immunol* 2007;179:4272–4282.
29. Hegmans JP, Hemmes A, Hammad H, Boon L, Hoogsteden HC, Lambrecht BN. Mesothelioma environment comprises cytokines and T-regulatory cells that suppress immune responses. *Eur Respir J* 2006;27:1086–1095.
30. Kettunen E, Nicholson AG, Nagy B, Wikman H, Seppanen JK, Stjernvall T, Ollikainen T, Kinnula V, Nordling S, Hollmen J, *et al.* L1CAM, INP10, P-cadherin, tPA and ITGB4 over-expression in malignant pleural mesotheliomas revealed by combined use of cDNA and tissue microarray. *Carcinogenesis* 2005;26:17–25.
31. Dufour JH, Dziejman M, Liu MT, Leung JH, Lane TE, Luster AD. IFN-gamma-inducible protein 10 (IP-10; CXCL10)-deficient mice reveal a role for IP-10 in effector T cell generation and trafficking. *J Immunol* 2002;168:3195–3204.
32. Kieseier BC, Tani M, Mahad D, Oka N, Ho T, Woodroofe N, Griffin JW, Toyka KV, Ransohoff RM, Hartung HP. Chemokines and chemokine receptors in inflammatory demyelinating neuropathies: a central role for IP-10. *Brain* 2002;125:823–834.
33. Liu L, Huang D, Matsui M, He TT, Hu T, Demartino J, Lu B, Gerard C, Ransohoff RM. Severe disease, unaltered leukocyte migration, and reduced IFN-gamma production in CXCR3−/− mice with experimental autoimmune encephalomyelitis. *J Immunol* 2006;176:4399–4409.
34. Kohyama N, Shinohara Y, Suzuki Y. Mineral phases and some reexamined characteristics of the International Union Against Cancer standard asbestos samples. *Am J Ind Med* 1996;30:515–528.
35. Scheule RK, Holian A. Immunologic aspects of pneumoconiosis. *Exp Lung Res* 1991;17:661–685.
36. Uber CL, McReynolds RA. Immunotoxicology of silica. *Crit Rev Toxicol* 1982;10:303–319.
37. Steenland K, Goldsmith DF. Silica exposure and autoimmune diseases. *Am J Ind Med* 1995;28:603–608.
38. Nishimura Y, Miura Y, Maeda M, Kumagai N, Murakami S, Hayashi H, Fukuoka K, Nakano T, Otsuki T. Impairment in cytotoxicity and expression of NK cell- activating receptors on human NK cells following exposure to asbestos fibers. *Int J Immunopathol Pharmacol* 2009;22:579–590.
39. Nishimura Y, Maeda M, Kumagai N, Hayashi H, Miura Y, Otsuki T. Decrease in phosphorylation of ERK following decreased expression of NK cell-activating receptors in human NK cell line exposed to asbestos. *Int J Immunopathol Pharmacol* 2009;22:879–888.
40. Tossavainen A, Karjalainen A, Karhunen PJ. Retention of asbestos fibers in the human body. *Environ Health Perspect* 1994;102:253–255.
41. Dodson RF, O'Sullivan MF, Huang J, Holiday DB, Hammar SP. Asbestos in extrapulmonary sites: omentum and mesentery. *Chest* 2000;117:486–493.
42. Uibu T, Vanhala E, Sajantila A, Lunetta P, Makela-Bengs P, Goebeler S, Jantti M, Tossavainen A. Asbestos fibers in para-aortic and mesenteric lymph nodes. *Am J Ind Med* 2009;52:464–470.
43. Noonan CW, Pfau JC, Larson TC, Spence MR. Nested case-control study of autoimmune disease in an asbestos-exposed population. *Environ Health Perspect* 2006;114:1243–1247.
44. Murakami S, Nishimura Y, Maeda M, Kumagai N, Hayashi H, Chen Y, Kusaka M, Kishimoto T, Otsuki T. Cytokine alteration and speculated immunological pathophysiology in silicosis and asbestos-related diseases. *Environ Health Prev Med* 2009;14:216–222.
45. Nishimoto N. Interleukin-6 as a therapeutic target in candidate inflammatory diseases. *Clin Pharmacol Ther* 2010;87:483–487.

46. Nowak AK, Lake RA, Kindler HL, Robinson BW. New approaches for mesothelioma: biologics, vaccines, gene therapy, and other novel agents. *Semin Oncol* 2002;29:82–96.
47. Fitzpatrick DR, Peroni DJ, Bielefeldt-Ohmann H. The role of growth factors and cytokines in the tumorigenesis and immunobiology of malignant mesothelioma. *Am J Respir Cell Mol Biol* 1995;12:455–460.
48. Diehl S, Anguita J, Hoffmeyer A, Zapton T, Ihle JN, Fikrig E, Rincon M. Inhibition of Th1 differentiation by IL-6 is mediated by SOCS1. *Immunity* 2000;13:805–815.
49. Mantovani A, Allavena P, Sica A, Balkwill F. Cancer-related inflammation. *Nature* 2008;454:436–444.
50. Maniati E, Soper R, Hagemann T. Up for mischief? IL-17/Th17 in the tumour microenvironment. *Oncogene* 2010;29:5653–5662.

Reduction of CXC Chemokine Receptor 3 in an *In Vitro* Model of Continuous Exposure to Asbestos in a Human T-Cell Line, MT-2

Megumi Maeda[1], Yasumitsu Nishimura[1], Hiroaki Hayashi[1], Naoko Kumagai[1], Ying Chen[1], Shuko Murakami[1], Yoshie Miura[3], Jun-ichi Hiratsuka[2], Takumi Kishimoto[4], and Takemi Otsuki[1]

[1]Department of Hygiene, and [2]Department of Radiation Oncology, Kawasaki Medical School, Okayama, Japan; [3]Division of Molecular and Clinical Genetics, Department of Molecular Genetics, Medical Institute of Bioregulation, Kyushu University, Fukuoka, Japan; and [4]Department at Okayama Rosai Hospital, Okayama, Japan

Because patients with silicosis who are chronically exposed to silica particles develop not only pulmonary fibrosis, but also complications involving autoimmune diseases such as rheumatoid arthritis and systemic sclerosis, exposure to asbestos may affect the human immune system. This immunologic effect may impair antitumor immune function because cancer complications such as lung cancer and malignant mesothelioma are found in patients exposed to asbestos. To elucidate the antitumor immune status caused by $CD4^+$ T cells exposed to asbestos, an *in vitro* T-cell model of long-term and low-level exposure to chrysotile asbestos was established from a human adult T-cell leukemia virus–1–immortalized human polyclonal T cell line, MT-2, and the resulting six sublines showed resistance to asbestos-induced apoptosis after more than 8 months of continuous exposure. The results of DNA microarray analysis showed that the expression of 139 genes was altered by long-term and low-level exposure to asbestos, and the profile was almost similar among the six sublines when compared with the original MT-2 cells that had never been exposed to asbestos. Pathway and network analysis indicated a down-regulation of IFN-γ signaling and expression of CXC chemokine receptor 3 (CXCR3) in the sublines, whereas ELISA and flow cytometry analysis demonstrated a reduction in Th1-related IFN-γ production and cell-surface CXCR3 expression. These findings suggest that chronic exposure to asbestos may reduce antitumor immune status in $CD4^+$ T cells, and that an *in vitro* T-cell model may be useful in identifying molecules related to the impairment of antitumor immune function.

Keywords: asbestos; malignant mesothelioma; CXCR3; IFN-γ

Exposure to asbestos (i.e., chrysotile, crocidolite, or amosite) leads to the development of asbestos-related diseases such as asbestos-related pleural plaque (PP) and malignant mesothelioma (MM) (1–3). Both diseases arise from exposure to asbestos, but MM has a poor prognosis, whereas PP is benign. Given that asbestos-related MM possesses a latency period ranging from 20–50 years, the peak of annual deaths from these diseases is predicted to occur around 2030 in Japan (4). Many investigations sought to elucidate the mechanisms underlying these diseases, and reports show that asbestos induces DNA damage and apoptosis in alveolar epithelial and mesothelial cells through a process mediated by reactive oxygen and nitrogen species of the mitochondrial dysfunction pathway (5–10).

CLINICAL RELEVANCE

We show that long-term and low-level exposures to asbestos decrease the expression of Th1-related molecules (CXCR3, IFN-γ, and CXCL10/IP10) in the $CD4^+$ T-cell line, MT-2, suggesting that exposure to asbestos may induce an impairment of antitumor immune responses. Therefore, our findings may be of use in detecting patients exposed to asbestos, identifying prognostic factors, and designing therapeutic devices to prevent the reduction of antitumor immune function found in immunocompetent cells exposed to asbestos.

MM is caused by exposure to asbestos, including conditions of long-term and low-level exposure. We reported that exposure to asbestos decreases the cytotoxicity of human natural killer (NK) cells, and that the cytotoxicity of NK cells is impaired in patients with MM (11, 12), suggesting that long-term and low-level exposures to asbestos may lead to a reduction of antitumor immune function. On the other hand, we showed that high-level exposures to asbestos induced the apoptosis of $CD4^+$ T cells in peripheral blood mononuclear cells *in vitro* because of activation-induced cell death (13, 14). Therefore, in an effort to determine whether long-term and low-level exposures of human immune cells to asbestos can induce a reduction in antitumor immune function, we developed an *in vitro* experimental model of chronic exposure to asbestos (chrysotile), using a human T-cell leukemia virus type–1 (HTLV-1)–immortalized human polyclonal T-cell line, MT-2 (15, 16), and we successfully established an asbestos-induced, apoptosis-resistant subline (MT-2Rst) (17). Because the original MT-2 cells (MT-2Org) constitute an HTLV-1–immortalized cell line, this line can continue to divide for many generations. In previous studies, we showed that long-term and low-level exposures to chrysotile induced an up-regulation of Src-family kinase–mediated IL-10 production, with a subsequent activation of the signal transducer and activator of transcription 3 (STAT3), and an overexpression of the antiapoptotic protein Bcl-2, located downstream from STAT3 (17). In addition, short-term and high-level exposures to chrysotile promoted the production of reactive oxygen species (ROS) and triggered apoptosis via a caspase-dependent mitochondrial pathway in the original MT-2 cells (MT-2Org) (18). These mechanisms are summarized in Figure 1.

We found that patients with MM manifest a high expression of *Bcl-2* in peripheral $CD4^+$ T cells (17), a high level of IL-10 and transforming growth factor (TGF)-β1 in plasma, and the multiple overrepresentation of the T-cell receptor Vβ in peripheral $CD3^+$ T cells (19, 20). Therefore, an analysis of the immunologic effects

(*Received in original form May 26, 2010 and in final form November 16, 2010*)

This study was supported by Special Coordination Funds for Promoting Science and Technology grant H18-1-3-3-1 (Comprehensive Approach on Asbestos-Related Diseases), grants from the Ministry of Education, Culture, Sports, Science and Technology of Japan (18390186, 19659153, 19790411, 20390178, and 22700933), and Kawasaki Medical School Project Grants (18-209T, 19-205Y, and 20-210O).

Correspondence and requests for reprints should be addressed to Megumi Maeda, Ph.D., Department of Hygiene, Kawasaki Medical School, 577 Matsushima, Kurashiki, Okayama 7010192, Japan. E-mail: mmaeda@med.kawasaki-m.ac.jp

Am J Respir Cell Mol Biol Vol 45. pp 470–479, 2011
Originally Published in Press as DOI: 10.1165/rcmb.2010-0213OC on December 10, 2010
Internet address: www.atsjournals.org

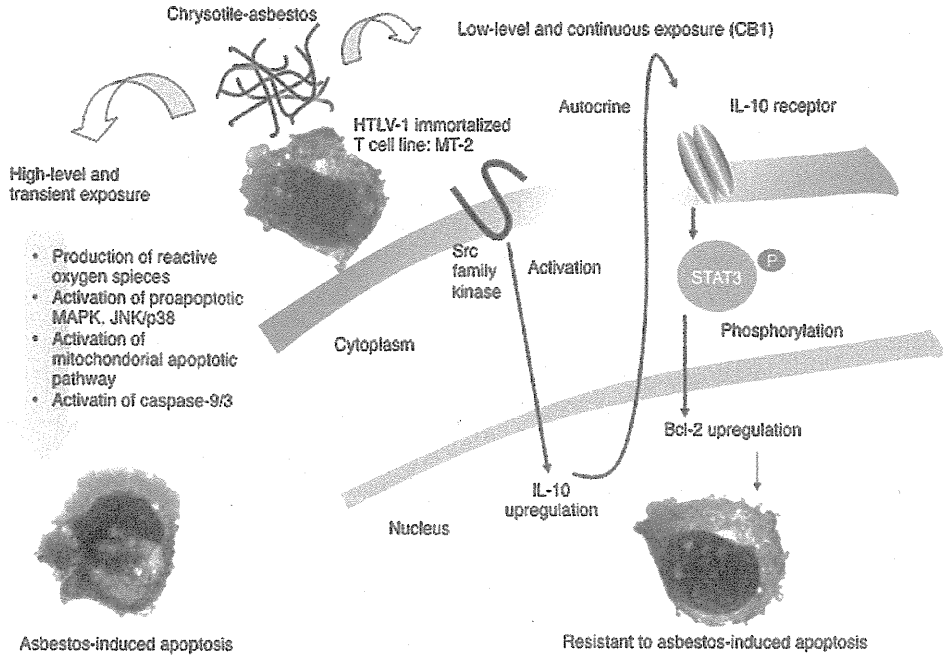

Figure 1. Schematic representation of molecular mechanism leading to resistance of MT-2Rst cells to asbestos-induced apoptosis. MT-2Rst cells continuously exposed to low-level chrysotile-B (CB) for more than 8 months showed resistance against asbestos-induced apoptosis, accompanied by the up-regulation of Src-family kinases, IL-10, signal transducer and activator of transcription 3 (STAT3), and Bcl-2, as previously reported (17, 18). HTLV-1, human T-cell leukemia virus type–1; JNK, c-Jun N-terminal kinase; MAPK, mitogen-activated protein kinase.

of asbestos on experimental T-cell models may help explain the reduced antitumor immune function in patients with MM.

Here, we investigated differences in gene expression between MT-2Org and six independent asbestos-induced, apoptosis-resistant sublines (MT-2Rsts) in an effort to identify genes altered by long-term and low-dose exposures to asbestos in T cells. Because three of the sublines were exposed to chrysotile-A (CA) and the other three were exposed to chrysotile-B (CB), they are designated as MT-2CA1–3 and MT-2CB1–3 (the initial MT-2Rst was CB1), respectively. Using these *in vitro* models of low-level and continuous exposure to asbestos, we found a down-regulation of Th1-type molecules such as CXC chemokine receptor 3 (CXCR3), chemokine (C-X-C motif) ligand 10 (CXCL10)/IFN-γ–induced protein 10 kD (IP10), and IFN-γ in MT-2Rsts cells.

These findings may useful in detecting patients exposed to asbestos, in identifying prognostic factors, and in designing therapeutic devices to prevent the reduction of antitumor immune function found in immunocompetent cells exposed to asbestos.

MATERIALS AND METHODS

Cell Lines and Asbestos

MT-2Org and MT-2Rsts cells were passaged many times in RPMI-1640 medium supplemented with 10% FBS, streptomycin, and penicillin at 37°C, and maintained in a humidified atmosphere of 5% CO_2. The International Union against Cancer standard CA and CB were kindly provided by the Department of Occupational Health at the National Institute for Occupational Health of South Africa (21). Chrysotile asbestos is composed of $Mg_3Si_2O_5(OH)_4$. CA from Zimbabwe contains 2% fibrous anthophyllite, although CB from Canada does not contain any fibrous impurities.

Real-Time RT-PCR

Real-time RT-PCR was performed using the SYBER Green method (TaKaRa, Shiga, Japan) with the Mx3000P QPCR System (Agilent Technologies, Inc., Santa Clara, CA), as previously described (17), to amplify CXCR3, chemokine (C-C motif) ligand 4 (CCL4)/macrophage inflammatory protein-1β (Mip-1β), and CC chemokine receptor 5 (CCR5). We used the primers CXCR3 forward (ACACCTTCCTG CTCCACCTA), CXCR3 reverse (GTTCAGGTAGCGGTCAAAGC), CCL4/MIP-1β forward (GAAAACCTCTTTGCCACCAA), CCL4/MIP-1β reverse (TCACTGGGATCAGCACAGAC), CCR5 forward (TAGTCATCTTGGGGCTGGTC), and CCR5 reverse (TGTAGGGA GCCCAGAAGAGA).

Flow Cytometry

Cells were stained with fluorescent conjugated antibodies for 30 minutes at 4°C. After washing with PBS, cells were analyzed on a flow cytometer (FACSCalibur; BD Biosciences, Franklin Lakes, NJ). The antibody used in this study was CXCR3-PE (clone 1C6; BD Biosciences Pharmingen, San Diego, CA).

ELISA

MT-2Org and MT-2Rsts cells (1×10^5/ml) were cultured in 24-well plates for 72 hours. The culture supernatants were then collected and assessed for the production of IFN-γ and CXCL10/IP10 by immunoassay, using Quantikine ELISA kits (R&D Systems, Minneapolis, MN).

DNA Microarray Analysis

Total RNA was isolated using the RNeasy Mini Kit (Qiagen GmbH, Hilden, Germany), and the quality of the RNA was assessed by examining the integrity of ribosomal RNA peaks, using an Agilent 2100 Bioanalyzer (Agilent Technologies, Inc.). Purified RNA (0.5 μg) was reverse transcribed using moloney murine leukemia virus reverse transcriptase (Agilent Technologies, Inc.) and a T7-oligo(-dT) promoter primer. After synthesis of the cDNA second strand, this product was employed to generate labeled complementary RNA (cRNA), using T7 RNA polymerase with cyanine 3–cytidine triphosphate (Low RNA Input Fluorescent Linear Amplification Kit; Agilent Technologies, Inc.). Labeled cRNA (1.5 μg) was then fragmented and hybridized to a 60-mer oligonucleotide microarray containing approximately 41,000 human genes (Human Whole Genome Oligo Microarray; Agilent Technologies, Inc.) for 17 hours at 65°C. After washing, the array was scanned using an Agilent DNA microarray scanner.

Data analysis was performed using Genespring (Agilent Technologies, Inc.). For statistical evaluation, expression profiles were normalized for the MT-2Org cell expression ratio to unity. After the removal of saturated and low-signal genes, genes that were twofold up-regulated or down-regulated in MT-2Rsts cells compared with MT-2Org cells were listed. The resultant signal information was analyzed using the Student t test ($P < 0.05$), and was clustered based on correlation coefficients. The resulting sets of differentially expressed genes were examined by pathway and network analysis, using the MetaCore Analytical Suite (http://www.genego.com; GeneGo, St. Joseph, MI).

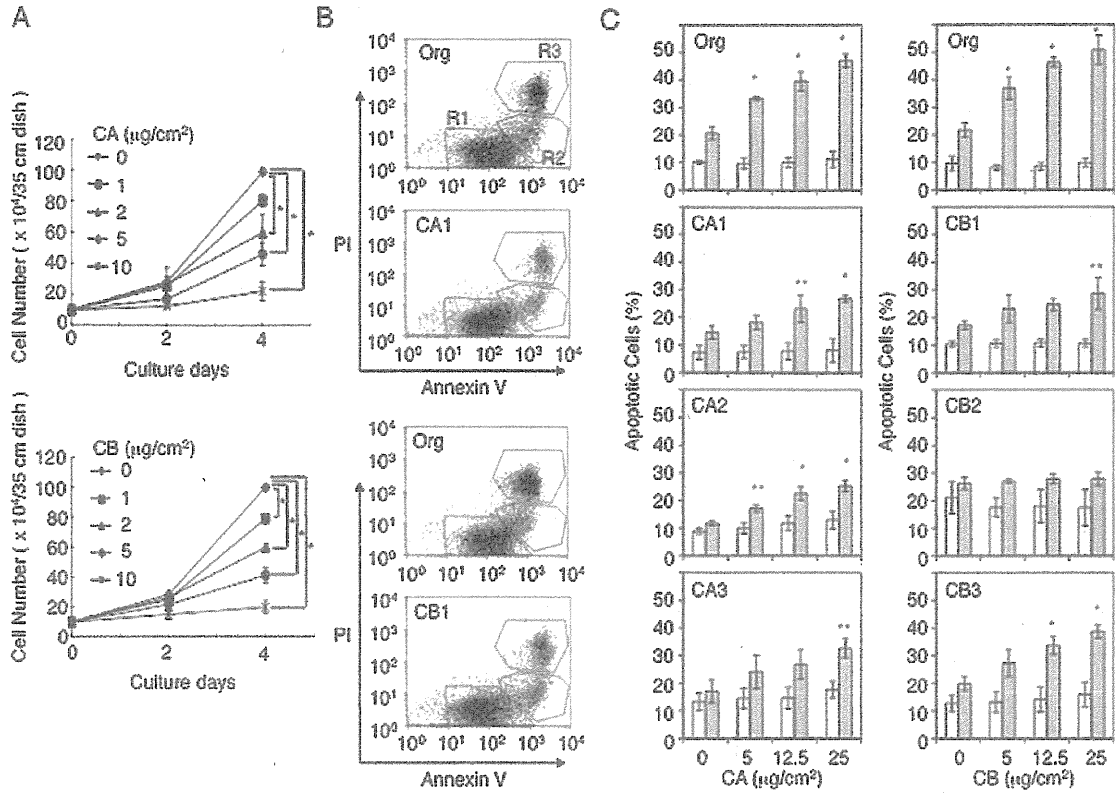

Figure 2. Original MT-2 (MT-2Org) cells acquire resistance to chrysotile-induced apoptosis by long-term and low-level exposures to chrysotile. (*A*) MT-2Org (Org) cells (1×10^5/2 ml) were cultured in the absence or presence of 1, 2, 5, or 10 μg/cm² chrysotile-A (CA) (*top*) or CB (*bottom*) in a 35-mm dish for 2 or 4 days. The number of viable cells was determined using the trypan blue dye exclusion test. (*B, C*) MT-2Org and MT-2Rsts (CA1, CA2, CA3, CB1, CB2, and CB3) cells (1×10^5/ml) were cultured in the absence or presence of 5, 12.5, or 25 μg/cm² CA or CB in 24-well plates. After 24 hours, apoptotic cells were detected by staining with Annexin V–FITC and propidium iodide, and stained cells were analyzed using FACS (FACS profiles shown in *B*). Region 1 (R1) represents viable cells (Annexin V-/PI-). Region 2 (R2) contains early apoptotic cells (Annexin V+/PI-). Region 3 (R3) includes late apoptotic cells (Annexin V+/PI+). (*C*) Percentages of apoptotic cells. *Open bars* and *gray bars* show (R2/(R1 + R2 + R3)) and ((R2 + R3)/(R1 + R2 + R3)), respectively. Data shown are the mean ± SD of three independent experiments. *P* values were obtained using Dunnett's test. $^*P < 0.01$. $^{**}P < 0.05$.

Statistical Analysis

Dunnett's test was performed to determine statistical differences between each experimental group and the control group.

RESULTS

Establishment of Six MT-2Rsts Cells (CA1–3 and CB1–3)

As we reported previously (17, 18), we initially established CB1 cells. Therefore, the other five independent MT-2Rsts cells continuously exposed to CA or CB were established according to a similar method. As shown in Figure 2A, the growth of MT-2Org cells was inhibited in a dose-dependent manner by culturing with CA or CB. This growth inhibition was confirmed by the appearance of apoptosis, as reported previously (17, 18), and as demonstrated in Figures 2B and 2C. All cultures for the establishment of MT-2Rsts cells were initiated in the presence of 2 μg/cm² CA or CB, at which stage the proliferation of MT-2Org cells was inhibited by half (Figure 2A). After 8–12 months of culture with CA or CB, MT-2Rsts cells began to exhibit a reduced apoptotic fraction when these cells were cultured with various concentrations of CA or CB (Figure 2C). Thus, we determined that six MT-2Rsts cells representing the acquisition of resistance to asbestos-induced apoptosis had been established, and these cells were designated CA1–3 and CB1–3. In this study, to identify those genes involved in the reduction of antitumor immune functions induced by exposure to asbestos, we used these six MT-2Rsts cells for DNA microarray analysis.

Gene Expression in MT-2Rsts Cells Altered by Chronic Exposure to Chrysotile

To examine alterations in gene expression by chronic exposure to chrysotile, DNA microarray analysis was performed with MT-2Org and MT-2Rsts cells. As listed in Table 1, the expression of 139 genes was altered (84 were up-regulated, and 55 were down-regulated) significantly (greater than twofold changes), and most were categorized in cellular components, biological processes, and molecular function groups by gene ontology analysis (data not shown). As shown in Figure 3, clustering analysis using these 139 genes revealed that the gene expression pattern was obviously different between MT-2Org and MT-2Rsts cells, and gene expression patterns were similar among all six MT-2Rsts cells, although small differences were evident. These results indicated that the changes in gene expression of MT-2Org cells are similarly induced by chronic exposure to CA and CB, suggesting that MT-2Rsts cells would be useful in further analyzing the immunologic effects of chrysotile asbestos.

Pathway and Network Analysis Using the MetaCore System

In an effort to identify genes related to the suppression of antitumor immunity among the 139 genes identified, expression

TABLE 1. GENES WITH AT LEAST A TWOFOLD DIFFERENCE BETWEEN MT-2ORG AND MT-2RSTS AT $P < 0.05$

Description	Genes	Accession Numbers
Down-regulated in MT-2Rsts compared with MT-2Org		
Solute carrier family 15, member 3	*SLC15A3*	NM_016582
Stomatin	*STOM*	NM_198194
Nedd4 family interacting protein 1	*NDFIP1*	NM_030571
Creatine kinase, brain	*CKB*	NM_001823
Tripartite motif–containing 22	*TRIM22*	NM_006074
Apolipoprotein C–I	*APOC1*	NM_001645
Forkhead box O1	*FOXO1*	NM_002015
Chromosome 1 open reading frame 218	*C1orf218*	NM_019049
Solute carrier family 6 (neurotransmitter transporter, taurine), member 6	*SLC6A6*	AB209172
c-mer proto-oncogene tyrosine kinase	*MERTK*	NM_006343
Interferon regulatory factor 9	*IRF9*	NM_006084
Asparaginase-like–1	*ASRGL1*	BC021295
Ankyrin repeat and death domain–containing 1A	*ANKDD1A*	AK075298
Protein phosphatase 1, regulatory (inhibitor) subunit 16B	*PPP1R16B*	NM_015568
Secreted protein, acidic, cysteine-rich (osteonectin)	*SPARC*	NM_003118
Chromosome 5 open reading frame 30	*C5orf30*	NM_033211
Stromal antigen 3	*STAG3*	NM_012447
Apolipoprotein L, 6	*APOL6*	AK074645
Chromosome 5 open reading frame 40	*C5orf40*	NM_001001343
CXXC finger 5	*CXXC5*	NM_016463
RNase, RNase A family, 1 (pancreatic)	*RNASE1*	NM_198232
Eukaryotic translation initiation factor 4 γ, 3	*EIF4G3*	NM_003760
Leukemia inhibitory factor (cholinergic differentiation factor)	*LIF*	NM_002309
Radial spoke head 1 homologue (*Chlamydomonas*)	*RSPH1*	NM_080860
cDNA DKFZp564D0472	*TOMM22*	AL110179
X-linked Kx blood group (McLeod syndrome)	*XK*	NM_021083
Caspase 2 and receptor-interacting serine-threonine kinase 1 domain containing adaptor with death domain	*CRADD*	NM_003805
Chromosome 13 open reading frame 15	*C13orf15*	NM_014059
An acute myeloid leukemia protein (486 bp)	*aml1*	X90980
Serine propidium iodide Kazal type 5–like 3	*SPINK5L3*	AK001520
Transmembrane and coiled-coil domain family 2	*TMCC2*	NM_014858
Von Willebrand factor	*VWF*	NM_000552
Acid phosphatase–like 2	*ACPL2*	NM_152282
Interferon-induced protein with tetratricopeptide repeats 2	*IFIT2*	NM_001547
Chemokine (C-C motif) ligand 4	*CCL4*	NM_002984
Napsin A aspartic peptidase	*NAPSA*	NM_004851
Hypothetical gene supported by AK125122	*FLJ13137*	AK125122
G-protein–coupled receptor 56	*GPR56*	NM_201525
Zinc finger CCCH-type containing 12D	*ZC3H12D*	AK127932
Similar to ciliary rootlet coiled-coil, rootletin	*LOC285188*	XM_209505
Membrane-associated ring finger (C3HC4) 3	*MARCH3*	NM_178450
Sequence 155 from Patent WO0220754	*AX721195*	AX721195
Protein kinase C, β1	*PRKCB1*	NM_002738
Interleukin 28A (interferon, λ2)	*IL28A*	NM_172138
DKFZP564O0823 protein	*DKFZP564O0823*	NM_015393
AF032119 hCASK {*Homo sapiens*;}, partial (13%)	*THC2443571*	THC2443571
Chromosome 19 open reading frame 38	*C19orf38*	XM_172995
Chemokine (C-X-C motif) receptor 3	*CXCR3*	NM_001504
Sema domain, transmembrane domain (TM), and cytoplasmic domain, (semaphorin) 6A	*SEMA6A*	NM_020796
Deleted in esophageal cancer 1	*DEC1*	BC030567
Phosphatidylinositol 3,4,5-trisphosphate–dependent Ras-related C3 botulinum toxin substrate 1 exchanger 1	*PREX1*	NM_020820
Breast cancer antiestrogen resistance 3	*BCAR3*	NM_003567
Myeloid cell nuclear differentiation antigen	*MNDA*	NM_002432
Integrin, β7	*ITGB7*	NM_000889
Hypothetical protein LOC199725	*LOC199725*	AK023628
Up-regulated in MT-2Rsts compared with MT-2Org		
Hypothetical LOC728701	*LOC728701*	BC011779
Mediator complex subunit 19	*MED19*	NM_153450
Norrie disease (pseudoglioma)	*NDP*	NM_000266
Protein phosphatase 6, regulatory subunit 1	*SAPS1*	NM_014931
Phosphoprotein enriched in astrocytes 15	*PEA15*	NM_003768
cDNA clone: 6386006	*BU587941*	BU587941
Hypothetical protein FLJ11348	*AK002210*	AK002210
FLJ00217 protein	*AK074144*	AK074144
cDNA clone: 5451514	*BM045853*	BM045853
F-box protein 2	*FBXO2*	NM_012168
cDNA clone: 1917130	*SSR2*	AI344752
AF4/FMR2 family, member 3	*AFF3*	NM_002285
Breakpoint cluster region	*BCR*	NM_021574
cDNA clone CS0DM002YA18	*CR608907*	CR608907

(*Continued*)

TABLE 1. (CONTINUED)

Description	Genes	Accession Numbers
Myc associated factor X dimerization protein 1	*MXD1*	NM_002357
cDNA MR0-RT0026-160401-104-h09 RT0026	*BI009763*	BI009763
Glutamate receptor interacting protein and coiled-coil domain containing 2	*GCC2*	NM_181453
Transmembrane emp24-like trafficking protein 10 (yeast) pseudogene	*TMED10P*	AJ004914
Special AT-rich sequence-binding protein homeobox 1	*SATB1*	NM_002971
Zinc finger CCCH-type containing 7A	*ZC3H7A*	NM_014153
Toll interacting protein	*TOLLIP*	NM_019009
cDNA FLJ13707 fis, clone PLACE2000347	*STAMBP*	AK023769
Ninein (GSK3B interacting protein)	*NIN*	NM_016350
Melanoma inhibitory activity family, member 3	*MIA3*	AK096526
Ras-related protein 1 GTPase-activating protein	*RAP1GAP*	NM_002885
Elongation factor Tu GTP binding domain containing 1	*EFTUD1*	NM_024580
Suppressor of Ty, domain containing 1 (*Saccharomyces cerevisiae*)	*SPTY2D1*	NM_194285
Hepatoma-derived growth factor, related protein 3	*HDGFRP3*	NM_016073
RNA binding motif protein 22	*RBM22*	NM_018047
Calcium/calmodulin-dependent serine protein kinase interacting protein 2	*CASKIN2*	NM_020753
Ras association (RalGDS/AF-6) and pleckstrin homology domains 1	*RAPH1*	NM_213589
Hypothetical protein LOC286272	*LOC286272*	AK000939
Transmembrane protease, serine 3	*TMPRSS3*	NM_032401
Coiled-coil domain containing 66	*CCDC66*	NM_001012506
Solute carrier family 45, member 4	*SLC45A4*	AB032952
cDNA clone: 3948082	*NOS1*	BC010126
Iroquois homeobox 5	*IRX5*	NM_005853
Organic solute transporter–β	*OSTbeta*	NM_178859
Hypothetical protein FLJ10404	*FLJ10404*	NM_019057
Regulating synaptic membrane exocytosis 3	*RIMS3*	NM_014747
Chorionic gonadotropin, β-polypeptide 1	*CGB1*	NM_033377
Secreted frizzled-related protein 1	*SFRP1*	NM_003012
Cysteine-rich secretory protein Limulus factor C, Coch-5b2 and Lgl1 domain–containing 2	*CRISPLD2*	BC007689
Protein phosphatase 1F (PP2C domain containing)	*PPM1F*	NM_014634
Steroidogenic acute regulatory protein-related lipid transfer (START) domain–containing 13	*STARD13*	NM_178006
Phospholipase C, β2	*PLCB2*	NM_004573
Glucosyltransferases, Rab-like GTPase activators and Myotubularins domain–containing 1C	*GRAMD1C*	NM_017577
cDNA clone: 998I221826	*BX119852*	BX119852
Replication protein A4, 34 kD	*RPA4*	NM_013347
Calcium-binding protein 7	*CABP7*	NM_182527
Golgin-like hypothetical protein LOC440321	*FLJ32679*	NM_001012452
Leucine-rich repeat–containing 2	*LRRC2*	NM_024512
Solute carrier family 10 (sodium/bile acid cotransporter family), member 1	*SLC10A1*	NM_003049
Tryptophan-aspartic acid repeat domain 33	*WDR33*	NM_018383
cDNA clone: 277235	*N47124*	N47124
Phosphoinositide-3–kinase, regulatory subunit 5	*PIK3R5*	NM_014308
Insulin-like growth factor binding protein 3	*IGFBP3*	NM_001013398
Dystrophin	*dystrophin*	S71486
Growth factor receptor bound protein 2-associated binding protein 2	*GAB2*	NM_012296
Carbonic anhydrase II	*CA2*	NM_000067
A kinase anchor protein 12	*AKAP12*	NM_144497
cDNA clone: 450936	*AA704712*	AA704712
Insulin-like growth factor 2 mRNA binding protein 2	*IGF2BP2*	NM_006548
Cystatin A (stefin A)	*CSTA*	NM_005213
Septin 1	*SEPT1*	NM_052838
Tight junction protein 1 (zona occludens 1)	*TJP1*	NM_003257
Coiled-coil domain containing 88A	*CCDC88A*	NM_018084
cDNA DKFZp686J1595	*BX538057*	BX538057
Chromosome 5 open reading frame 39	*C5orf39*	NM_001014279
Calcium-binding protein 39-like	*CAB39L*	NM_030925
Transmembrane protein 56	*TMEM56*	NM_152487
Tryptophan-tryptophan domain containing oxidoreductase	*WWOX*	NM_130844
FLJ35767 protein	*FLJ35767*	NM_207459
Riboflavin kinase	*RFK*	NM_018339
Stress-associated endoplasmic reticulum protein family member 2	*SERP2*	NM_001010897
Dehydrogenase/reductase member 9	*DHRS9*	NM_005771
Teashirt zinc finger homeobox 1	*TSHZ1*	NM_005786
Nance-Horan syndrome-like 1	*NHSL1*	AB037778
Solute carrier family 39 (zinc transporter), member 6	*SLC39A6*	NM_012319
Zinc finger, Cysteine-cysteine-histidine-cysteine domain–containing 2	*ZCCHC2*	BC006340
Zinc-binding alcohol dehydrogenase domain–containing 2	*ZADH2*	NM_175907
Pentraxin-related gene, rapidly induced by IL-1β	*PTX3*	NM_002852
Family with sequence similarity 124B	*FAM124B*	NM_024785
Forkhead box F2	*FOXF2*	NM_001452

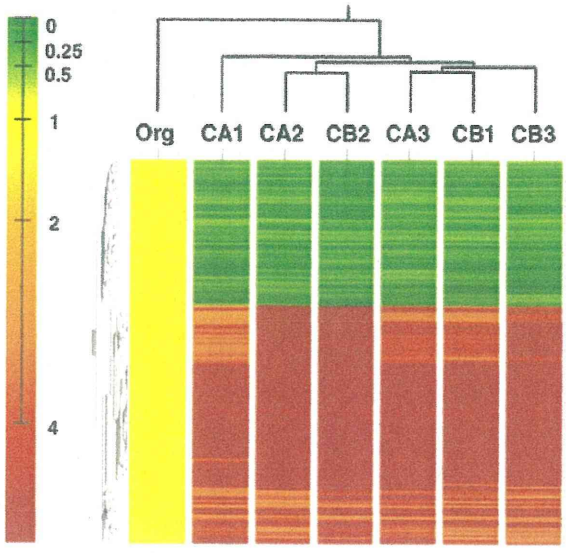

Figure 3. Clustering analysis of 139 genes reveals differences between MT-2Org and MT-2Rsts cells. Expression is scaled so that *green* represents low expression, and *red* represents high expression.

data were processed by the MetaCore system, which allows the visualization of microarray data on canonical pathways and the construction of gene networks using pathway and network analysis. The top 30 results of the pathway analysis are listed in Table 2. We focused on the suppression of the IFN-γ signaling pathway, because the production of IFN-γ was shown to decrease in CB1 cells compared with MT-2Org cells (17), and IFN-γ is considered one of the most important cytokines for organizing tumor rejection by immunocompetent cells. The expression of two genes, IFN regulatory factor 9 (*IRF9*) and IFN-stimulated gene factor–3 (*ISGF3*), was significantly reduced in all MT-2Rsts cells exposed continuously to CA or CB (Figure 4). In addition, the build networks from the 139 genes indicated that the decreased expression of CXCR3 in all MT-2Rsts cells was regulated by *IRF9* through CXCL10/IP-10 (Figure 5). Therefore, the cell-surface expression of CXCR3 was thought to be important among the cellular and molecular alterations in MT-2Rsts cells continuously exposed to asbestos.

Decline of Th1-Type CXCR3 Expression, IFN-γ Production, and CXCL10/IP10 Production in MT-2Rsts Cells Chronically Exposed to Chrysotile Asbestos

Because the expression of CXCR3 and production of IFN-γ are known to be induced by T-cell activation and lead to the enhancement of antitumor immune function (22), we investigated the expression of the Th1-type chemokine receptor CXCR3 and cytokine IFN-γ. As shown in Figure 6A, the cell-surface expression of CXCR3 was examined in gated live cells on MT-2Org and MT-2Rsts cells. All MT-2Rsts cells showed a reduction of cell-surface CXCR3-positive cells, although no significant difference was evident between MT-2Org and CB2 cells, as indicated by real-time RT-PCR (Figure 6B). Furthermore, all MT-2Rsts cells showed less production of IFN-γ compared with MT-2Org cells (Figure 7A). These findings support the notion that the down-regulation of Th1-type molecules CXCR3 and IFN-γ is important in recognizing the immunologic effect of asbestos.

As shown in Figure 7B, the production of the Th1-type CXCR3 ligand CXCL10/IP10 was also significantly reduced in all MT-2Rsts cells compared with MT-2Org cells. In addition, another Th1-type chemokine, *CCL4/ MIP-1*β mRNA, was also expressed at low concentrations in all MT-2Rsts cells compared

TABLE 2. PATHWAY RESULTS

Map	*P* values[a]
1. Phosphatidylinositol-3,4,5-trisphosphate signaling in B lymphocytes	5.22E-03
2. IFN-α/β signaling pathway	9.05E-03
3. Regulation of lipid metabolism G–α(q) regulation of lipid metabolism	1.55E-02
4. Inhibitory action of lipoxins on superoxide production in neutrophils	1.95E-02
5. Angiotensin signaling via signal transducers and activators of transcription	1.95E-02
6. Transcription factor Tubby signaling pathways	2.62E-02
7. Transcription regulation of granulocyte development	3.46E-02
8. Apoptosis and survival–β-2 adrenergic receptor antiapoptotic action	4.71E-02
9. Membrane trafficking and signal transduction of G-α (i) heterotrimeric G-protein	5.30E-02
10. Gap junctions	9.35E-02
11. G-protein–β/γ signaling cascades	1.01E-01
12. Macrophage migration inhibitory factor, the neuroendocrine-macrophage connector	1.32E-01
13. α-2 adrenergic receptor regulation of ion channels	1.40E-01
14. Antiviral actions of interferons	1.65E-01
15. Calcium signaling	1.74E-01
16. Extracellular signal–regulated kinase interactions: inhibition of extracellular signal–regulated kinases	1.82E-01
17. G-protein–mediated regulation mitogen-activated protein kinase-extracellular signal–regulated kinase signaling	1.91E-01
18. Endothelin receptor type B signaling	1.91E-01
19. A1 receptor signaling	2.00E-01
20. A3 receptor signaling	2.00E-01
21. G-protein–mediated regulation p38 and c-Jun N-terminal kinase signaling	2.00E-01
22. Inducible costimulator-Inducible costimulator ligand pathway in T-helper cells	2.09E-01
23. Histamine H1 receptor signaling in the interruption of cell-barrier integrity	2.17E-01
24. Inhibitory action of lipoxins on neutrophil migration	2.17E-01
25. Histamine signaling in dendritic cells	2.35E-01
26. Activation of protein kinase C via G-protein–coupled receptor	2.35E-01
27. Inositol 1,4,5-triphosphate signaling	2.44E-01
28. Role of vitamin D receptor in regulation of genes involved in osteoporosis	2.80E-01
29. IFN-γ signaling pathway	2.89E-01
30. G protein-coupled receptors in platelet aggregation	3.42E-01

[a]*P* values is calculated by comparing the number of interest genes that participate in a given pathway, relative to the total number of occurrences of these genes in all pathway annotations stored in the Metacore database.

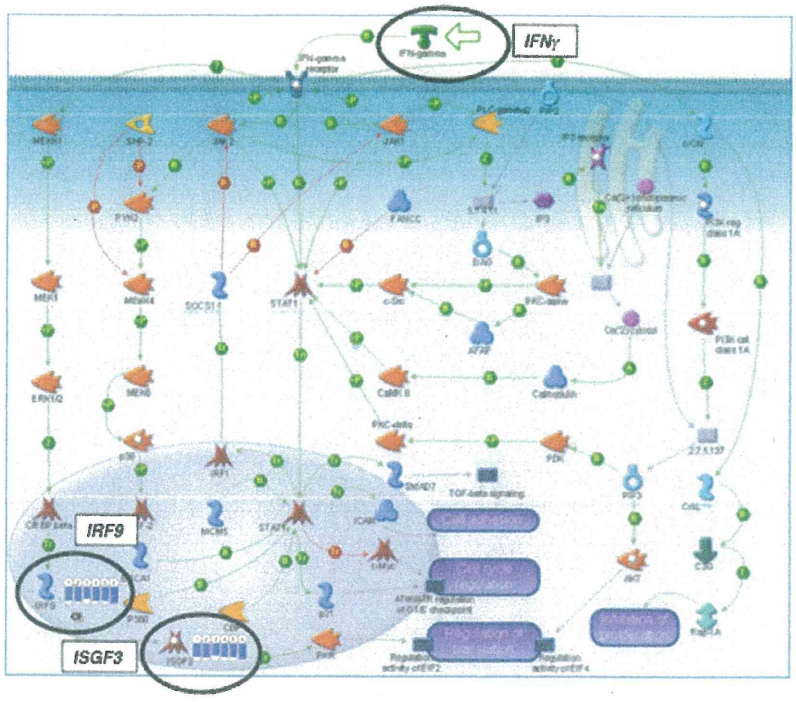

Figure 4. IFN-γ signaling canonical pathway analysis shows that the expression of *IRF9* and *ISGF3* is down-regulated in MT-2Rsts cells. *Blue thermometers* indicate down-regulation. Numbers indicate cell line names (2, CA1; 3, CA2; 4, CA3; 5, CB1; 6, CB2; 7, CB3).

with MT-2Org cells (Table 1 and Figure 7C). However, CCR5, the Th1-type receptor for CCL4/MIP-1β, was not reduced significantly through the expression of mRNA in MT-2Rsts cells (Figure 7C). These results indicate that a continuous exposure of MT-2Org cells to asbestos altered the expression of Th1-related chemokines (CXCL10/IP10 and CCL4/MIP-1β) and chemokine receptors (CXCR3).

DISCUSSION

Pneumoconiosis is an occupational and restrictive set of lung diseases caused by the inhalation of dust, often in mines (23–26), and typically including silicosis and asbestosis. Silicosis is caused by the inhalation of crystalline silica dust, and is marked by inflammation and scarring in the form of nodular lesions in the upper lobes of lungs. On the other hand, asbestosis is a chronic inflammatory and fibrotic medical condition affecting the parenchymal tissue of the lungs, and is caused by the inhalation and retention of asbestos fibers. It usually occurs after high-intensity or long-term exposure to asbestos, particularly in individuals working on the production or end-use of products containing asbestos (23–26). Patients with silicosis suffer not only from respiratory dysfunction, but sometimes from complications involving autoimmune diseases such as rheumatoid arthritis

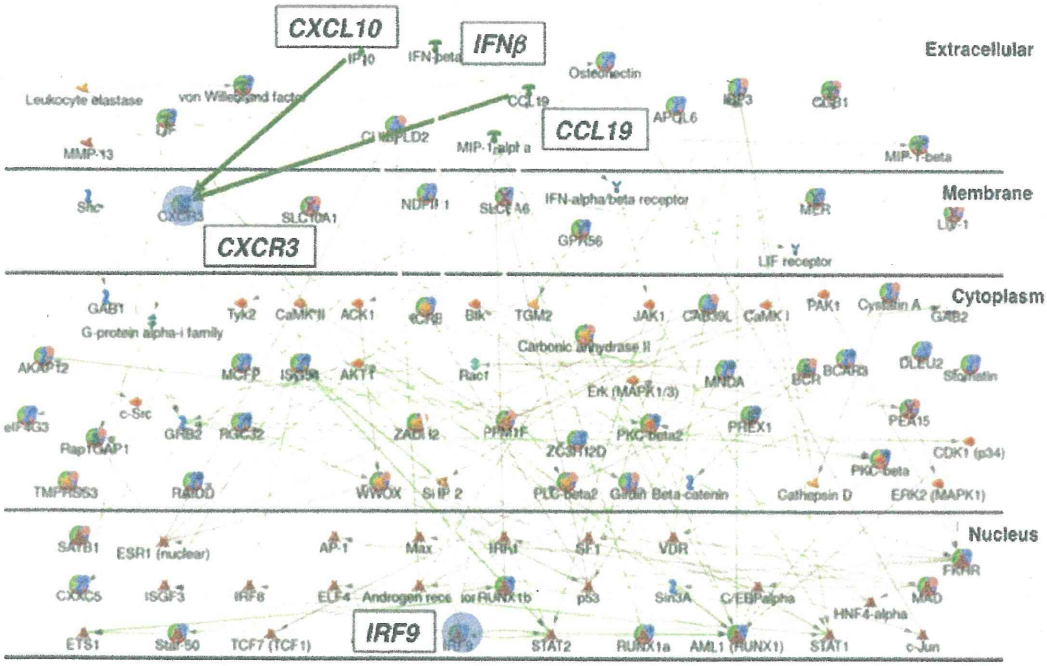

Figure 5. Network analysis indicates that down-regulation of *CXCR3* is regulated by *IRF9*. *Blue circles* indicate reduced genes. *Green arrows* and *gray arrows* indicate positive and unspecified effects, respectively.

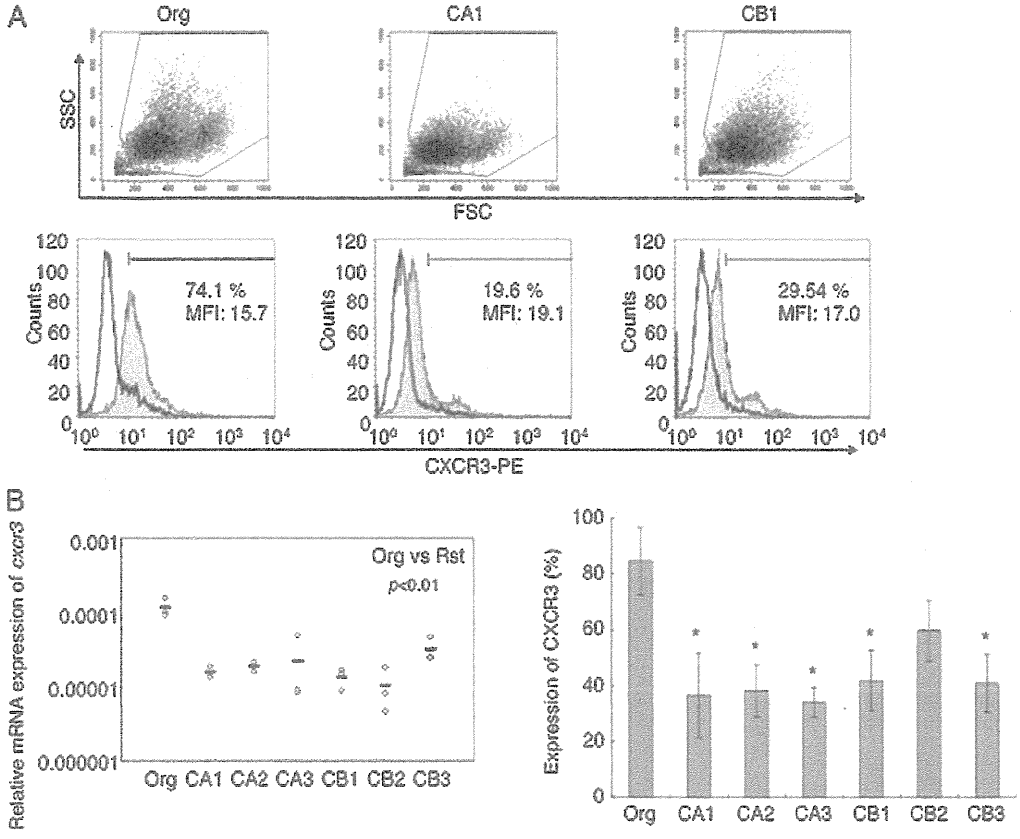

Figure 6. Chronic exposure to chrysotile inhibits the expression of CXCR3 in MT-2Rsts cells. (*A*) Representative FACS profiles of cell-surface CXCR3 expression on MT-2Org, CA1, and CB1. Living cells were gated, based on forward scatter (FSC) and side scatter (SSC) (*upper dot plot*). Gated cells were analyzed for the expression of CXCR3 (*lower histogram*). Peaks are shown in unstained control samples (*solid lines*) and stained samples (*gray peaks*). Percentages of CXCR3-positive cells and the mean fluorescence intensity (MFI) of gated cells are indicated in the histogram. (*B*) Total RNA was isolated, and the relative mRNA expression of *CXCR3* was estimated by real-time RT-PCR (*left*). Graph at *right* depicts the ratios of cell-surface CXCR3-positive cells in MT-2Org and MT-2Rsts. Results represent the mean ± SD of three independent experiments. *P* values were obtained using Dunnett's test. $^{*}P < 0.01$. $^{**}P < 0.05$.

(known as Caplan's syndrome), systemic sclerosis, and antineutrophil cytoplasmic autoantibody–related vasculitis/nephritis (26–28). However, the most important complication in patients exposed to asbestos involves the occurrence of cancers, such as lung cancer and MM. In particular, MM is known to be caused by low-level and long-term exposures to asbestos (29–31).

We have been studying the mechanisms of dysregulation of autoimmunity caused by exposure to silica, and reported on alterations in Fas/CD95 and related molecules (32, 33), the activation of T cells by silica via the activation of antigen-presenting cells such as dendritic cells and monocyte/macrophage-lineage cells (34), and a reduction of regulatory T-cell function in the peripheral $CD4^+CD25^+$ fraction (35). On the other hand, asbestos is a mineral silicate that contains magnesium, iron, and calcium, with a core of SiO_2 (36, 37). Thus, asbestos may affect human immunocompetent cells because silica can modify human immunity (32–35). In view of these facts, if we think about the medical complications of a population exposed to silica or asbestos, patients may exhibit a reduced antitumor immune function because of developing cancers possessing a long-term latent phase (20–50 years) after an initial exposure to asbestos (29–31).

Therefore, we previously investigated the effects of asbestos on NK cells, and reported impairment in the cytotoxicity and expression of NK cell–activating receptor NKp46 and a decrease in the phosphorylation of the extracellular signal–regulated kinase signaling molecule in NK cells exposed to asbestos (11, 12). We also studied the effects of asbestos in relation to $CD8^+$ cytotoxic T cells, and found impairment in the differentiation and proliferation of these cells, the details of which will be reported in the future.

In regard to $CD4^+$ T cells, we established an *in vitro* cell line model of low-level and continuous exposure to asbestos (17, 18). MT-2 cells (15, 16) were chosen and underwent an initial screening for growth inhibition by culturing with asbestos to detect sensitivity to asbestos-induced apoptosis, because cell lines derived from leukemia and lymphoma may already possess alterations in many cellular and molecular events due to transformation. Moreover, chrysotile was initially used to analyze the immunologic effects of asbestos, because this fiber is used widely throughout the world.

First, we reported that high-dose and transient exposure induced apoptosis in MT-2 cells, caused by the production of ROS, the activation of proapoptotic c-Jun N-terminal kinase and p38 signaling molecules in the mitogen-activated protein kinase pathway, and the activation of the mitochondrial apoptotic pathway, as shown in Figure 1 (18). These findings were also evident when CA including 2% fibrous anthophyllite was used for exposure, as described in alveolar epithelial and pleural mesothelial cells (5–10). Next, we established a subline exposed to long-term and low-level CB (17). This subline showed the acquisition of resistance to asbestos-induced apoptosis through an activation of Src-family kinases, the up-regulation of IL-10 production, the activation of STAT3, and the up-regulation of Bcl-2, as shown in Figure 1 (17). Furthermore, the expression of *Bcl-2* in $CD4^+$ T cells from patients with MM was significantly up-regulated compared with that in healthy donors (17). However, because we ran only one trial to establish the low-level and continuous exposure model, we cannot confirm whether the findings in this subline represent general responses.

Therefore, we established five other independent sublines involving long-term and low-level exposure to chrysotile, because the other altered molecules should be identified for a better understanding of the asbestos-induced reduction of antitumor immune function. As shown in Figures 2 and 7A, all

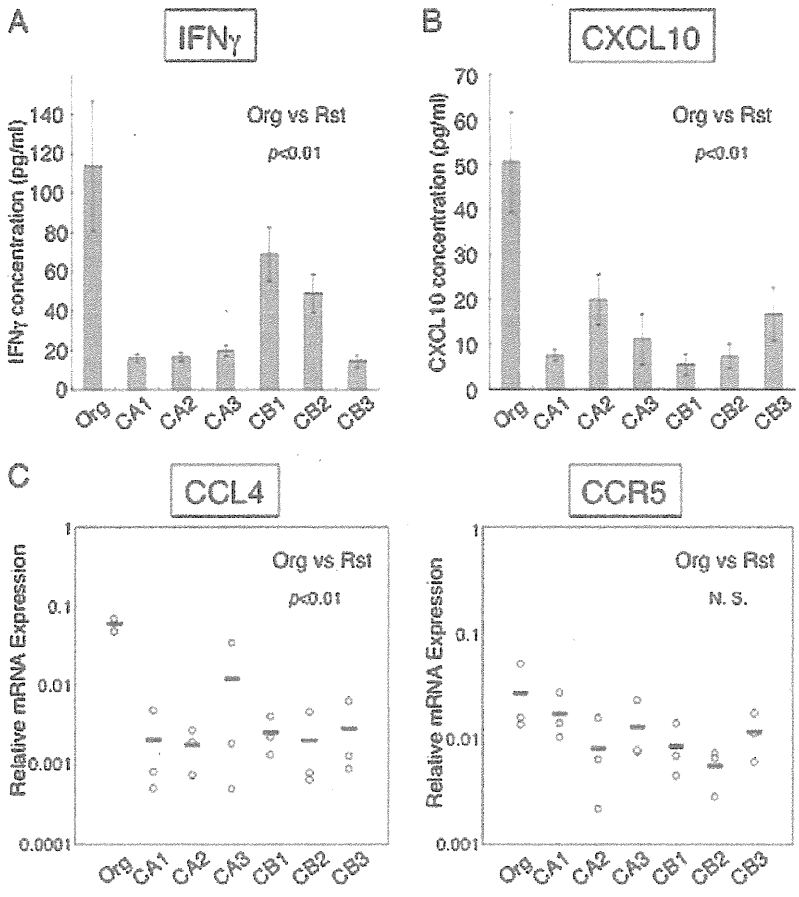

Figure 7. Continuous exposure to chrysotile decreases Th1-type cytokine IFN-γ and chemokine CXCL10/IP10 production in MT-2Rsts cells. (*A, B*) MT-2Org and MT-2Rsts cells were cultured for 72 hours. Culture supernatants were then collected and assessed for IFN-γ and CXCL10/IP10 production by ELISA. (*C*) The mRNA expressions of the Th1-type chemokine CCL4/MIP-1β and the receptor CCR5 were estimated using real-time RT-PCR. Results represent the mean ± SD of three independent experiments. *P* values were obtained using Dunnett's test. $^{*}P < 0.01$. $^{**}P < 0.05$.

six sublines, including the initial subline (CB1), exhibited a resistance to asbestos-induced apoptosis and a reduction of IFN-γ production, in a manner similar to that shown in previous studies (17). These findings indicate that the cellular and molecular alterations found in these sublines can be regarded as the universal immunologic effects of asbestos in T cells, although these findings should be confirmed using freshly isolated lymphocytes from both healthy donors and patients with MM exposed to asbestos.

An exhaustive analysis using DNA microarray, pathway, and network analyses identified the suppression of the Th1-type IFN-γ signaling pathway and CXCR3 expression. These alterations were confirmed by the decreased production of IFN-γ and decreased cell-surface expression of CXCR3 in all cell lines. IFN-γ is an antitumor cytokine, and it is used for the treatment of various cancers to enhance the antitumor activity of T cells, NK cells, and natural killer T cells (38, 39). In addition, the chemokine receptor CXCR3 is a G-protein–coupled seven-transmembrane receptor expressed on various lymphocytes, including T cells, B cells, and NK cells, and it binds to IFN-γ–inducible chemokines such as CXCL9/MIG, CXCL10/IP10, and CXCL11/I-TAC that recruit leukocytes to inflammatory sites such as tumors (40). In the case of $CD4^+$ T cells, CXCR3 is preferentially expressed on IFN-γ–producing Th1/effector T cells. Our previous study showed that original MT-2 cells exhibit a high-level production of inflammatory cytokine IFN-γ, TNF-α, and IL-6, whereas sublines produce an anti-inflammatory cytokine IL-10 at a high concentration (17), suggesting that the Th1/effector T-cell–like characteristics of MT-2Org cells may easily be suppressed by long-term and low-level exposures to chrysotile, although the mRNA expression of Th1-type CCR5 (41) was not inhibited significantly (Figure 7C). Moreover, all six sublines showed a down-regulation of Th1-type chemokine CXCL10/IP10 and CCL4/MIP-1β. Generally, both CXCL10/IP10 and CCL4/MIP-1β are secreted by activated T cells, and contribute to the attraction of Th1/effector T cells (41, 42). Therefore, the suppression of Th1-type molecules such as CXCR3, IFN-γ, CXCL10/IP10, and CCL4/MIP-1β in sublines continuously exposed to chrysotile can be considered evidence of asbestos-induced cellular and molecular alterations in immunocompetent cells. Exposure to asbestos seems to modify antitumor immune function and local (pulmonary) inflammatory reactions because of changes in the expression and production levels of cytokines, chemokines, and chemokine receptors in immune competent cells.

These findings may provide an explanation for the rapid progression of asbestos-related cancers, although further research is needed to confirm whether these alterations in cell-line models arise in freshly isolated human lymphocytes derived from healthy donors and patients with PP or MM.

Author Disclosure: None of the authors has a financial relationship with a commercial entity that has an interest in the subject of this manuscript.

Acknowledgments: We thank Tamayo Hatayama, Minako Kato, Naomi Miyahara, Shoko Yamamoto, Misao Kuroki, Keiko Kimura, Yoshiko Yamashita, and Tomoko Sueishi for technical assistance.

References

1. Pan XL, Day HW, Wang W, Beckett LA, Schenker MB. Residential proximity to naturally occurring asbestos and mesothelioma risk in California. *Am J Respir Crit Care Med* 2005;172:1019–1025.
2. Cugell DW, Kamp DW. Asbestos and the pleura: a review. *Chest* 2004; 125:1103–1117.
3. Miserocchi G, Sancini G, Mantegazza F, Chiappino G. Translocation pathways for inhaled asbestos fibers. *Environ Health* 2008;7:4.

4. Murayama T, Takahashi K, Natori Y, Kurumatani N. Estimation of future mortality from pleural malignant mesothelioma in Japan based on an age-cohort model. *Am J Ind Med* 2006;49:1–7.
5. Upadhyay D, Kamp DW. Asbestos-induced pulmonary toxicity: role of DNA damage and apoptosis. *Exp Biol Med (Maywood)* 2003;228: 650–659.
6. Panduri V, Surapureddi S, Soberanes S, Weitzman SA, Chandel N, Kamp DW. P53 mediates amosite asbestos–induced alveolar epithelial cell mitochondria–regulated apoptosis. *Am J Respir Cell Mol Biol* 2006;34:443–452.
7. Upadhyay D, Panduri V, Kamp DW. Fibroblast growth factor–10 prevents asbestos-induced alveolar epithelial cell apoptosis by a mitogen-activated protein kinase–dependent mechanism. *Am J Respir Cell Mol Biol* 2005;32:232–238.
8. Mossman BT. Introduction to serial reviews on the role of reactive oxygen and nitrogen species (ROS/RNS) in lung injury and diseases. *Free Radic Biol Med* 2003;34:1115–1116.
9. Kamp DW, Panduri V, Weitzman SA, Chandel N. Asbestos-induced alveolar epithelial cell apoptosis: role of mitochondrial dysfunction caused by iron-derived free radicals. *Mol Cell Biochem* 2002;234–235: 153–160.
10. Jiang L, Nagai H, Ohara H, Hara S, Tachibana M, Hirano S, Shinohara Y, Kohyama N, Akatsuka S, Toyokuni S. Characteristics and modifying factors of asbestos-induced oxidative DNA damage. *Cancer Sci* 2008;99:2142–2151.
11. Nishimura Y, Miura Y, Maeda M, Kumagai N, Murakami S, Hayashi H, Fukuoka K, Nakano T, Otsuki T. Impairment in cytotoxicity and expression of NK cell-activating receptors on human NK cells following exposure to asbestos fibers. *Int J Immunopathol Pharmacol* 2009;22:579–590.
12. Nishimura Y, Maeda M, Kumagai N, Hayashi H, Miura Y, Otsuki T. Decrease in phosphorylation of ERK following decreased expression of NK cell–activating receptors in human NK cell line exposed to asbestos. *Int J Immunopathol Pharmacol* 2009;22:879–888.
13. Ueki A, Yamaguchi M, Ueki H, Watanabe Y, Ohsawa G, Kinugawa K, Kawakami Y, Hyodoh F. Polyclonal human T-cell activation by silicate *in vitro*. *Immunology* 1994;82:332–335.
14. Aikoh T, Tomokuni A, Matsukii T, Hyodoh F, Ueki H, Otsuki T, Ueki A. Activation-induced cell death in human peripheral blood lymphocytes after stimulation with silicate *in vitro*. *Int J Oncol* 1998;12:1355–1359.
15. Miyoshi I, Kubonishi I, Yoshimoto S, Shiraishi Y. A T-cell line derived from normal human cord leukocytes by co-culturing with human leukemic T-cells. *Gann* 1981;72:978–981.
16. Miyoshi I, Kubonishi I, Yoshimoto S, Akagi T, Ohtsuki Y, Shiraishi Y, Nagata K, Hinuma Y. Type C virus particles in a cord T-cell line derived by co-cultivating normal human cord leukocytes and human leukaemic T cells. *Nature* 1981;294:770–771.
17. Miura Y, Nishimura Y, Katsuyama H, Maeda M, Hayashi H, Dong M, Hyodoh F, Tomita M, Matsuo Y, Uesaka A, *et al.* Involvement of IL-10 and Bcl-2 in resistance against an asbestos-induced apoptosis of T cells. *Apoptosis* 2006;11:1825–1835.
18. Hyodoh F, Takata-Tomokuni A, Miura Y, Sakaguchi H, Hatayama T, Hatada S, Katsuyama H, Matsuo Y, Otsuki T. Inhibitory effects of antioxidants on apoptosis of a human polyclonal T-cell line, MT-2, induced by an asbestos, chrysotile-A. *Scand J Immunol* 2005;61:442–448.
19. Maeda M, Miura Y, Nishimura Y, Murakami S, Hayashi H, Kumagai N, Hatayama T, Katoh M, Miyahara N, Yamamoto S, *et al.* Immunological changes in mesothelioma patients and their experimental detection. *Clin Med Insights Circ Respir Pulmon Med* 2008;2:11–17.
20. Nishimura Y, Miura Y, Maeda M, Hayashi H, Dong M, Katsuyama H, Tomita M, Hyodoh F, Kusaka M, Uesaka A, *et al.* Expression of the T cell receptor Vbeta repertoire in a human T cell resistant to asbestos-induced apoptosis and peripheral blood T cells from patients with silica and asbestos-related diseases. *Int J Immunopathol Pharmacol* 2006;19:795–805.
21. Kohyama N, Shinohara Y, Suzuki Y. Mineral phases and some reexamined characteristics of the International Union against Cancer standard asbestos samples. *Am J Ind Med* 1996;30:515–528.
22. Luster AD, Leder P. IP-10, a -C-X-C- chemokine, elicits a potent thymus-dependent antitumor response *in vivo*. *J Exp Med* 1993;178: 1057–1065.
23. Abraham JL. Recent advances in pneumoconiosis: the pathologist's role in etiologic diagnosis. *Monogr Pathol* 1978;19:96–137.
24. Vallyathan NV, Green FH, Craighead JE. Recent advances in the study of mineral pneumoconiosis. *Pathol Annu* 1980;15:77–104.
25. Begin R, Cantin A, Masse S. Recent advances in the pathogenesis and clinical assessment of mineral dust pneumoconioses: asbestosis, silicosis and coal pneumoconiosis. *Eur Respir J* 1989;2:988–1001.
26. Scheule RK, Holian A. Immunologic aspects of pneumoconiosis. *Exp Lung Res* 1991;17:661–685.
27. Uber CL, McReynolds RA. Immunotoxicology of silica. *Crit Rev Toxicol* 1982;10:303–319.
28. Steenland K, Goldsmith DF. Silica exposure and autoimmune diseases. *Am J Ind Med* 1995;28:603–608.
29. Kannerstein M, Churg J, McCaughey WT. Asbestos and mesothelioma: a review. *Pathol Annu* 1978;13:81–129.
30. Kannerstein M, Churg J, McCaughey E, Selikoff IJ. Pathogenic effects of asbestos. *Arch Pathol Lab Med* 1977;101:623–628.
31. Craighead JE, Mossman BT. The pathogenesis of asbestos-associated diseases. *N Engl J Med* 1982;306:1446–1455.
32. Otsuki T, Miura Y, Nishimura Y, Hyodoh F, Takata A, Kusaka M, Katsuyama H, Tomita M, Ueki A, Kishimoto T. Alterations of Fas and Fas-related molecules in patients with silicosis. *Exp Biol Med (Maywood)* 2006;231:522–533.
33. Otsuki T, Maeda M, Murakami S, Hayashi H, Miura Y, Kusaka M, Nakano T, Fukuoka K, Kishimoto T, Hyodoh F, *et al.* Immunological effects of silica and asbestos. *Cell Mol Immunol* 2007;4:261–268.
34. Wu P, Hyodoh F, Hatayama T, Sakaguchi H, Hatada S, Miura Y, Takata-Tomokuni A, Katsuyama H, Otsuki T. Induction of CD69 antigen expression in peripheral blood mononuclear cells on exposure to silica, but not by asbestos/chrysotile-A. *Immunol Lett* 2005;98:145–152.
35. Wu P, Miura Y, Hyodoh F, Nishimura Y, Hatayama T, Hatada S, Sakaguchi H, Kusaka M, Katsuyama H, Tomita M, *et al.* Reduced function of $CD4^{+}25^{+}$ regulatory T cell fraction in silicosis patients. *Int J Immunopathol Pharmacol* 2006;19:357–368.
36. Pooley FD. Mineralogy of asbestos: the physical and chemical properties of the dusts they form. *Semin Oncol* 1981;8:243–249.
37. Stephens M, Gibbs AR, Pooley FD, Wagner JC. Asbestos induced diffuse pleural fibrosis: pathology and mineralogy. *Thorax* 1987;42: 583–588.
38. Rudge G, Barrett SP, Scott B, van Driel IR. Infiltration of a mesothelioma by IFN-gamma–producing cells and tumor rejection after depletion of regulatory T cells. *J Immunol* 2007;178:4089–4096.
39. Miller CH, Maher SG, Young HA. Clinical use of interferon-gamma. *Ann N Y Acad Sci* 2009;1182:69–79.
40. Rotondi M, Chiovato L, Romagnani S, Serio M, Romagnani P. Role of chemokines in endocrine autoimmune diseases. *Endocr Rev* 2007;28: 492–520.
41. Luther SA, Cyster JG. Chemokines as regulators of T cell differentiation. *Nat Immunol* 2001;2:102–107.
42. Loetscher M, Loetscher P, Brass N, Meese E, Moser B. Lymphocyte-specific chemokine receptor CXCR3: regulation, chemokine binding and gene localization. *Eur J Immunol* 1998;28:3696–3705.

Clinical Effectiveness of Boron Neutron Capture Therapy for a Recurrent Malignant Peripheral Nerve Sheath Tumor in the Mediastinum

Masayoshi Inoue, MD, PhD, Chun Man Lee, MD, PhD,† Koji Ono, MD, PhD,‡ Minoru Suzuki, MD, PhD,‡ Toshiteru Tokunaga, MD,* Yoshiki Sawa, MD, PhD,† and Meinoshin Okumura, MD, PhD**

A 70-year-old woman underwent extirpation of a malignant peripheral nerve sheath tumor, 4.5 × 2.0 cm in size, in the right supraclavicular fossa. Locoregional recurrence was found 10 months after operation (Figure 1). Although one course of systemic chemotherapy using cisplatin (80 mg/m^2 at day 1) and vinorelbine (25 mg/m^2 at days 1 and 8) was given, the recurrent tumor progressed. Because conventional radiotherapy is not effective for malignant peripheral nerve sheath tumor, boron neutron capture therapy (BNCT) was considered based on the subcutaneous mediastinal location. After institutional review board approval and securing the patient's written informed consent, accumulation of p-boronophenylalanine (BPA) in the tumor was confirmed using 18F-BPA positron emission tomography. Using simulation environment for radiation applications software program, fast neutron and γ-ray physical doses, compound biologic effectiveness- and relative biologic effectiveness-weighted doses, were calculated.

The patient underwent two courses of BNCT with an interval of 3 weeks. BPA-fructose was administered intravenously at a dose of 500 mg/kg just before irradiation. For the first course, the epithermal neutron irradiation was performed for 105 minutes. The dose distribution in the tumor ranged from 13.7 to 22.3 Gy-Eq and was 6.0 Gy-Eq to the skin. For the second course, the irradiation time was shortened to 51 minutes, because of the higher epithermal neutron flux. The dose delivered to the tumor ranged from 6.0 to 24.3 Gy-Eq and was 9.7 Gy-Eq to the skin.

Chest computed tomography scan 1 year after BNCT showed that the tumor size decreased from 6.2 × 4.0 cm to 4.6 × 3.2 cm in size (25% reduction), and stable disease was maintained for 24 months (Figure 2). Positron emission tomography-computed tomography 18 months after BNCT showed no uptake of 18F-fluorodeoxy glucose in the residual mass, suggesting no viability (Figure 3). Neuralgia of the right arm improved. Although temporary dysphagia because of an oral mucosa disorder was observed as a side effect, the patient's general quality of life was preserved. There is no evidence of recurrence 2 years after BNCT.

DISCUSSION

When ^{10}Boron absorbs thermal neutrons, α and ^{7}Lithium particles are generated.[1] BNCT selectively injures the tumor cells containing ^{10}Boron; it was suitable in this case with tumor invasion into the neighboring great vessels. Because the peak of thermal neutron flux is 3 cm beneath the tissue surface, its clinical applications have been limited to malignant melanomas and brain tumors. Kato et al.[2] reported its efficacy for head and neck malignancies. The indication was extended to metastatic liver tumor,[3] malignant mesothelioma,[4] and glioblastoma.[5] This is the first case of mediastinal tumor treated with BNCT.

The effect of BNCT is critically dependent on selective accumulation of ^{10}Boron compounds. The tumor/normal tissue ratio of the ^{10}Boron uptake was 2 in this case, while a ratio greater than 2.5 is preferable for selective treatment. BNCT might be a treatment option for subcutaneous mediastinal tumors, which is resistant to conventional irradiation.

REFERENCES

1. Barth RF, Coderre JA, Vicente MG, et al. Boron neutron capture therapy of cancer: current status and future prospects. *Clin Cancer Res* 2005; 11:3987–4002.
2. Kato I, Ono K, Sakurai Y, et al. Effectiveness of BNCT for recurrent head and neck malignancies. *Appl Radiat Isot* 2004;61:1069–1073.
3. Wittig A, Malago M, Collette L, et al. Uptake of two 10B-compounds in liver metastases of colorectal adenocarcinoma for extracorporeal irradiation with boron neutron capture therapy (EORTC Trial 11001). *Int J Cancer* 2008;122:1164–1171.
4. Suzuki M, Sakurai Y, Masunaga S, et al. Feasibility of boron neutron capture therapy (BNCT) for malignant pleural mesothelioma from a viewpoint of dose distribution analysis. *Int J Radiat Oncol Biol Phys* 2006;66:1584–1589.
5. Vos MJ, Turowski B, Zanella FE, et al. Radiologic findings in patients treated with boron neutron capture therapy for glioblastoma multiforme within EORTC trial 11961. *Int J Radiat Oncol Biol Phys* 2005;61:392–399.

*Department of General Thoracic Surgery, Osaka University Graduate School of Medicine, Suita, Osaka; †Medical Center for Translational Research, Osaka University Hospital, Suita, Osaka; and ‡Radiation Oncology Research Laboratory, Research Reactor Institute, Kyoto University, Kyoto, Japan.

Disclosure: The authors declare no conflicts of interest.

Address for correspondence: Meinoshin Okumura, MD, Department of General Thoracic Surgery, Osaka University Graduate School of Medicine, L5-2-2 Yamadaoka, Suita, Osaka 565-0781, Japan. E-mail: meinosin@thoracic.med.osaka-u.ac.jp

ISSN: 1556-0864/10/0512-2037

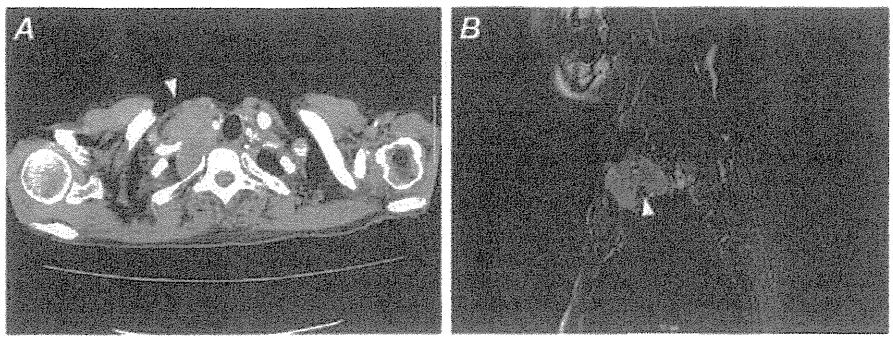

FIGURE 1. Chest computed tomography (CT) scan and magnetic resonance imaging (MRI) showing the recurrent lesion. *A*, Postoperative recurrence, 4.5 × 2.0 cm in size, is seen in the right subclavicular region (arrow head) in the follow-up CT scan 10 months after operation. *B*, Tumor invasion into the right subclavicular artery and brachiocephalic vein is seen (arrow head) in the sagittal view of MRI.

FIGURE 2. Chest computed tomography scan 1 year after boron neutron capture therapy shows shrinkage of the recurrent lesion after chemotherapy from 6.2 × 4.0 cm to 4.6 × 3.2 cm in size (25% reduction).

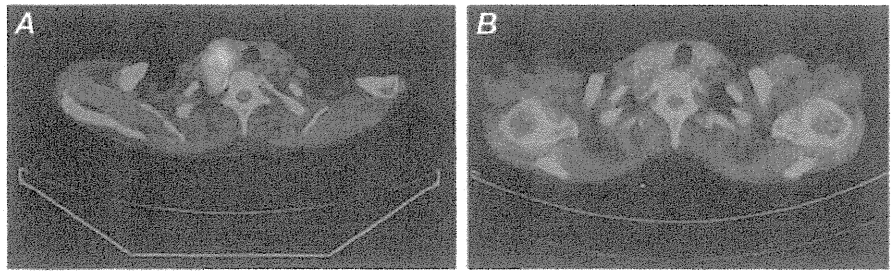

FIGURE 3. FDG-positron emission tomography (PET) shows the remarkable effect of boron neutron capture therapy (BNCT). *A*, PET-computed tomography (CT) before BNCT shows significant tumor uptake. *B*, Although a residual mass is seen, the FDG uptake is reduced to the background level 18 months after BNCT.

Published OnlineFirst October 21, 2011; DOI:10.1158/1078-0432.CCR-11-0868

Clinical Cancer Research

Early [^{18}F]Fluorodeoxyglucose Positron Emission Tomography at Two Days of Gefitinib Treatment Predicts Clinical Outcome in Patients with Adenocarcinoma of the Lung

Ryo Takahashi, Haruhiko Hirata, Isao Tachibana, et al.

Clin Cancer Res 2012;18:220-228. Published OnlineFirst October 21, 2011.

Published OnlineFirst October 21, 2011; DOI:10.1158/1078-0432.CCR-11-0868

Clinical Cancer Research

Imaging, Diagnosis, Prognosis

Early [^{18}F]Fluorodeoxyglucose Positron Emission Tomography at Two Days of Gefitinib Treatment Predicts Clinical Outcome in Patients with Adenocarcinoma of the Lung

Ryo Takahashi[1], Haruhiko Hirata[1], Isao Tachibana[1], Eku Shimosegawa[2], Atsuo Inoue[2], Izumi Nagatomo[1], Yoshito Takeda[1], Hiroshi Kida[1], Sho Goya[1], Takashi Kijima[1], Mitsuhiro Yoshida[1], Toru Kumagai[1], Atsushi Kumanogoh[1], Meinoshin Okumura[3], Jun Hatazawa[2], and Ichiro Kawase[4]

Abstract

Purpose: Positron emission tomography (PET) with [^{18}F]fluorodeoxyglucose (FDG) is increasingly used in early assessment of tumor response after chemotherapy. We investigated whether a change in [^{18}F]FDG uptake at 2 days of gefitinib treatment predicts outcome in patients with lung adenocarcinoma.

Experimental Design: Twenty patients were enrolled. [^{18}F]FDG-PET/computed tomographic (CT) scan was carried out before and 2 days after gefitinib treatment. Maximum standardized uptake values (SUV) were measured, and post-gefitinib percentage changes in SUV were calculated. Early metabolic response (SUV decline < −25%) was compared with morphologic response evaluated by CT scan and with progression-free survival (PFS).

Results: At 2 days of gefitinib treatment, 10 patients (50%) showed metabolic response, 8 had metabolic stable disease, and 2 had progressive metabolic disease. Percentage changes of SUV at 2 days were correlated with those of tumor size in CT at 1 month ($R^2 = 0.496$; $P = 0.0008$). *EGFR* gene was assessable in 15 patients, and of 12 patients with *EGFR* mutations, 8 showed metabolic response at 2 days and 6 showed morphologic response at 1 month. None of 3 patients with wild-type *EGFR* showed metabolic or morphologic response. Metabolic response at 2 days was not statistically associated with PFS ($P = 0.095$), but when a cutoff value of −20% in SUV decline was used, metabolic responders had longer PFS ($P < 0.0001$).

Conclusion: Early assessment of [^{18}F]FDG tumor uptake with PET at 2 days of gefitinib treatment could be useful to predict clinical outcome earlier than conventional CT evaluation in patients with lung adenocarcinoma. *Clin Cancer Res; 18(1); 220–8. ©2011 AACR.*

Introduction

Treatment of non–small cell lung cancer (NSCLC) has made remarkable progress in the last decade; the epidermal growth factor receptor (EGFR), which is expressed in more than 60% of patients with metastatic NSCLC and correlates with poor prognosis (1), has emerged as an important molecular target for advanced or recurrent NSCLC. Reversible EGFR tyrosine kinase inhibitors (TKI), gefitinib and erlotinib, were found to have antitumor activities in second- or third-line therapy (2–4). Objective responses with these agents were limited to a subpopulation of patients, which included never-smokers, women, East Asians, and patients with adenocarcinoma histology (4, 5). It was later shown that most of these responders harbor specific mutations or increased copy number in the gene encoding EGFR that enhances tyrosine kinase activity (6, 7). Indeed, gefitinib as first-line and single-agent therapy improved progression-free survival (PFS) of patients with NSCLC with the *EGFR* mutations when compared with standard chemotherapy (8–10). Although these genetic markers may be used to predict therapeutic response, they do not guarantee successful treatment as a portion of marker-positive patients did not respond to the EGFR TKIs, whereas a portion of marker-negative patients did respond (11). Moreover, a secondary mutation in the *EGFR* gene or amplification of *c-Met* negates the sensitizing effect, leading to acquired

Authors' Affiliations: Departments of [1]Respiratory Medicine, Allergy and Rheumatic Diseases, [2]Nuclear Medicine, and [3]General Thoracic Surgery, Osaka University Graduate School of Medicine; and [4]Osaka Prefectural Medical Center for Respiratory and Allergic Diseases, Osaka, Japan

Note: Supplementary data for this article are available at Clinical Cancer Research Online (http://clincancerres.aacrjournals.org/).

R. Takahashi and H. Hirata contributed equally to the work as the first authors.

Corresponding Author: Isao Tachibana, Department of Respiratory Medicine, Allergy and Rheumatic Diseases, Osaka University Graduate School of Medicine, 2-2 Yamada-oka, Suita, Osaka 565-0871, Japan. Phone: 81-6-6879-3833; Fax: 81-6-6879-3839; E-mail: itachi02@imed3.med.osaka-u.ac.jp

doi: 10.1158/1078-0432.CCR-11-0868

Published OnlineFirst October 21, 2011; DOI:10.1158/1078-0432.CCR-11-0868

Translational Relevance

It remains difficult to accurately predict clinical benefit of gefitinib in patients with non–small cell lung cancer (NSCLC). A recent basic study using a mouse model has shown that gefitinib induces a decrease of fluorodeoxyglucose (FDG) uptake within 48 hours in sensitive NSCLC tumors. We conducted a pilot study to validate the use of early FDG-positron emission tomography (PET) in clinical settings. Assessment of FDG uptake only after 2 days of gefitinib treatment was able to predict tumor response and progression-free survival. This early assessment could help to identify patients who will benefit from gefitinib therapy while allowing for rapid initiation of alternative strategies and minimizing critical adverse effects such as interstitial lung disease when gefitinib is ineffective.

resistance to the EGFR TKIs (12). Thus, it appears difficult to predict clinical benefit accurately only with these genetic biomarkers.

Positron emission tomography (PET) with [^{18}F]fluorodeoxyglucose (FDG) plays a role in the diagnosis and staging of lung cancer. It is based on high glucose metabolism in tumor cells that have an increased level of glucose transport protein expression and hexokinase activity. In addition to diagnosis and staging, [^{18}F]FDG-PET is increasingly used to assess tumor response and to predict outcome. A decrease in FDG uptake in sensitive tumor cells can be detected earlier than structural changes occur (13). This is the case especially in tumors treated with molecularly targeted drugs rather than with cytotoxic agents. In gastrointestinal stromal tumors (GIST), FDG-PET has been shown to be highly sensitive in detecting early response to imatinib mesylate, a small molecule that inhibits c-KIT. Decreases in FDG uptake were observed after 1 week of treatment, whereas volume responses evaluated on computed tomographic (CT) scan were small and developed more slowly (14, 15). In NSCLC, it has remained unknown that how EGFR TKIs downregulate FDG uptake after initiation of treatment in sensitive tumors. Recently, using a mouse xenograft model, Su and colleagues showed rapid decreases of tumor FDG uptake in sensitive xenografts within 48 hours of gefitinib treatment (16). They also found a decline in FDG uptake 24 to 48 hours before inhibition of proliferation and induction of apoptosis in a gefitinib-sensitive NSCLC cell line. A more recent preliminary study, which evaluated [^{18}F]FDG-PET in 5 patients with advanced NSCLC treated with gefitinib, suggested that FDG-PET may be able to predict the response. Patients exhibiting a partial response on CT evaluation already showed a mean of 61% decrease in FDG uptake at 2 days of therapy (17). Thus, further prospective studies are needed to confirm that [^{18}F]FDG-PET provides an early sensitive marker of the effectiveness of gefitinib in patients with NSCLC.

In the present study, we prospectively evaluated FDG-PET only after 2 days of gefitinib treatment in patients with lung adenocarcinoma to predict response and outcome. We used a combined PET/CT scan to provide correct anatomic registration of PET data.

Materials and Methods

Patients

Twenty patients with lung adenocarcinoma who received gefitinib treatment were enrolled from November 2007 to November 2009. Diagnosis was made either histologically or cytologically. Gefitinib at a dose of 250 mg once a day was administered orally 30 minutes after breakfast as the first EGFR tyrosine kinase inhibition therapy, until disease progression, unacceptable toxicity, or patient refusal. Eligibility criteria included an age of 20 years or more, unresectable stage or relapse after surgery, measurable disease, and Eastern Cooperative Oncology Group (ECOG) performance status of 0 to 2. The study protocol was approved by the Institutional Review Board of Osaka University Hospital, Osaka, Japan, and written informed consent was obtained from all patients.

EGFR mutation analysis

Mutation analysis of *EGFR* in exons 18, 19, 20, and 21 was conducted using biopsy specimens obtained at diagnosis. Genomic DNA was extracted and analyzed by peptide nucleic acid–locked nucleic acid PCR (PNA-LNA PCR) cramp method manufactured in Mitsubishi Chemical Medience Co., as previously described (18).

FDG-PET/CT

[^{18}F]FDG-PET/CT was conducted before (at baseline), 2 days, and 1 month after gefitinib administration using a GEMINI GXL scanner (Philips Medical Systems). Baseline scan was done within 14 days prior to the treatment. All patients were fasted for at least 4 hours before scanning. Their serum glucose levels were less than 150 mg/dL before FDG injection. One hour after the injection of 3.7 MBq/kg [^{18}F]FDG, patients were scanned from the head to the thigh. We calculated accurate [^{18}F]FDG uptake time for each patient and confirmed that there was no significant difference between any metabolic responders and nonresponders. After a 50-mAs low-dose CT scan for attenuation correction, emission scan was obtained in a 3-demensional acquisition mode at 11 to 12 bed positions with 2 min/bed speed. In-plane and axial field of view of the scanner were 576 mm and 180 mm, respectively. In-plane spatial resolution was 6.31 mm full width at half maximum (FWHM) at the center with 144 × 144 pixel size (4 × 4 × 4 mm^3/pixel). Images were reconstructed by line-of-response row-action maximum likelihood algorithm (LOR-RAMLA) method. After acquisition of the PET images, a diagnostic chest CT was conducted by a 16-row multidetector scanner in a helical mode with 120 kV of the tube voltage and 200 mAs of the effective tube current. CT gantry rotation time was 0.5 seconds with an axial field of view of 600 mm,

Published OnlineFirst October 21, 2011; DOI:10.1158/1078-0432.CCR-11-0868

producing 5-mm thick slices with a 512 × 512 matrix. Regions of interest were placed over the highest accumulation area, corresponding to tumor sites on the PET images. The maximal standardized uptake value (SUV) was determined as previously described (19).

Response assessment and follow-up

Among measurable lesions according to the Response Evaluation Criteria in Solid Tumors version 1.0 (RECIST 1.0; ref. 20) in fused mode of dual modality PET/CT, up to 5 lesions in order of [^{18}F]FDG uptake level were defined as target lesion on the baseline scan. [^{18}F]FDG uptake was evaluated as the SUV of the target lesions (21). The lowest SUV of target lesions was 1.6, which was still higher than the background (Table 1). On PET/CT at 2 days and 1 month of gefitinib administration, percentage changes in the sum of these SUVs of the target metabolic lesions were determined on the basis of the baseline scan, and time point metabolic response was defined according to the recommendations of the European Organization for Research and Treatment of Cancer (EORTC) PET study group (22). Complete metabolic response (CMR) was achieved when SUVs of all lesions were decreased to uptake equivalent to background. Partial metabolic response (PMR) was defined as percentage change of the sum of SUVs (ΔSUV%) < −25%, stable metabolic disease (SMD) was −25% ≤ ΔSUV% < +25%, and progressive metabolic disease (PMD) was defined as +25% ≤ ΔSUV% or when the extent of [^{18}F]FDG increased greater than 20% in the longest dimension or when new [^{18}F]FDG uptake appeared in metastatic lesions. In analysis of PFS, a cutoff value of −20%, instead of −25%, was also used to separate responders from nonresponders. Changes in tumor size of the same target lesions as [^{18}F]FDG uptake analysis and nontarget lesions were quantified on CT images from PET/CT data at 1 month by 2 of the authors blinded to the PET data, and time point overall response was classified according to RECIST 1.0. Percentage changes in the sum of the longest dimension (ΔCTsize%) of the target lesions were also determined and compared with ΔSUV%. On CT images at 2 days of gefitinib administration, all patients were with stable disease. Chest CT or radiograph was repeated every 4 weeks until disease progression, which was determined by RECIST 1.0. The overall responses classified at 1 month were not confirmed by the repeat assessments in this study.

Table 1. Patient characteristics at baseline

Characteristic	*N*
Total no. of patients	20
Sex	
Male	5
Female	15
Age, y	
Median	69
Range	58–83
ECOG performance status	
0	10
1	10
Smoking history	
Never	15
Ever	5
Clinical stage	
IIIA	2
IIIB	3
IV	15
No. of prior chemotherapy	
0	10
1	6
2	2
3	1
4	1
EGFR mutation status	
Exon 19	6
Exon 21	5
Exon 18	1
Wild-type	3
Not determined	1
Not tested	4
Baseline study	
No. of target lesions	
Median	2.5
Range	1–5
SUV of target lesions	
Median	5.9
Range	1.6–13.0
Size of target lesions, cm	
Median	2.0
Range	1.2–7.7

Statistical analysis

Data were analyzed using JMP statistical discovery software version 8.0.2 (SAS Institute). Correlation between ΔSUV% at 2 days and ΔCTsize% at 1 month was evaluated by Fisher ANOVA. Agreement between the EORTC recommendations–based metabolic response at 2 days and RECIST-based morphologic overall response at 1 month was evaluated using kappa statistic (23). PFS was measured from the first administration of gefitinib to documented progression or death of any cause. Overall survival (OS) was from the first administration of gefitinib to death of any cause. PFS and OS were estimated using the Kaplan–Meier method and compared by the 2-sided log-rank test (24). HRs were calculated using the Cox proportional hazards model. In multivariate Cox model analysis, metabolic response at 2 days and morphologic response at 1 month, significance of which was $P < 0.15$ in univariate analysis, were chosen as variable in addition to smoking history, which was previously shown to be a prognostic factor for patients with gefitinib-treated NSCLC (5). *EGFR* mutation status was not included because it was not determined or tested in 5 patients, and the number of patients with wild-type *EGFR* was only 3.

Published OnlineFirst October 21, 2011; DOI:10.1158/1078-0432.CCR-11-0868

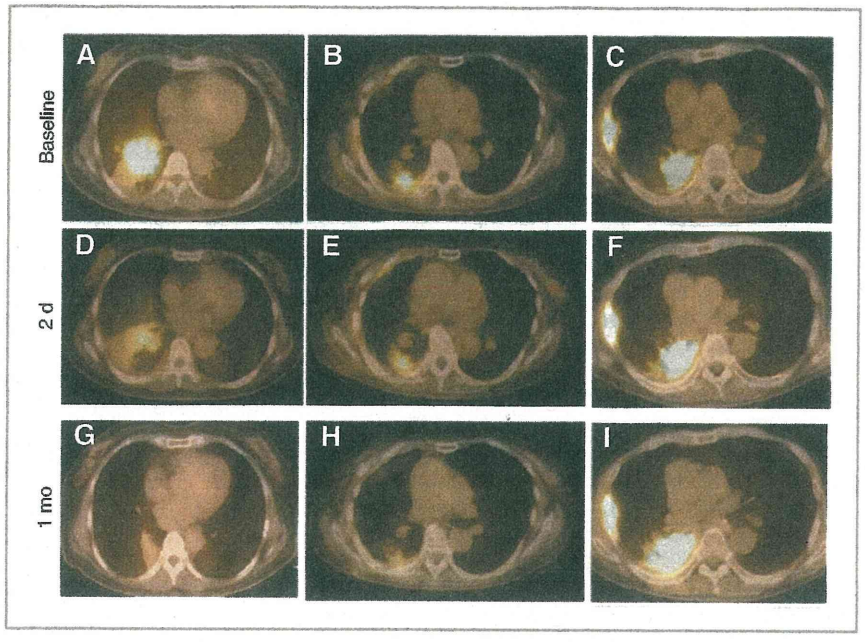

Figure 1. Pre- and posttreatment images of FDG-PET/CT scans of a 67-year-old female (A, D, and G) and a 75-year-old female (B, E, and H), who achieved partial response at 1 month (G and H, respectively), and an 81-year-old male (C, F, and I), who had progressive disease at 1 month (I) as assessed by RECIST 1.0. The first 2 patients already showed partial metabolic response at 2 days (D and E), and the third patient was assessed with progressive metabolic disease at 2 days (F).

Results

Patient characteristics

A total of 20 patients (15 females and 5 males) were enrolled in this study, underwent PET/CT for baseline assessment, and received gefitinib treatment. Nineteen were patients with adenocarcinoma and one with adenosquamous carcinoma. Fifteen patients (75%) had clinical stage IV disease. Five patients at clinical stage III were not treated with surgery or radiation due to the presence of malignant pleural effusion and complicating diseases. Ten were previously untreated and 10 had been treated with 1 to 4 chemotherapy regimens. Detailed patient characteristics are shown in Table 1. Median time between the baseline PET/CT and the start of gefitinib treatment was 4 days (range, 0–13 days), and no chemotherapy was administered during this period. A 77-year-old male patient did not complete PET/CT at 1 month because ground-glass opacity appeared on chest radiograph and gefitinib administration was discontinued at 6 days of treatment; this patient was excluded from later assessment. In all the other patients, gefitinib was continued to documented disease progression, and none of them received additional treatment without documented progression. Overall, early response at 2 days was assessed in 20 patients, and late response assessment at 1 month and PFS analysis were conducted in 19 patients.

Comparative analysis of metabolic and morphologic responses

Metabolic responses could be detected only at 2 days of treatment, when morphologic responses were still unrecognizable. Representative PET/CT images of responders and nonresponders during gefitinib treatment were shown in Fig. 1. Median percentage change of the sum of SUVs (ΔSUV%) of target lesions was −23%. Sixteen patients experienced ΔSUV% reduction ranging from −2% to −52% (Fig. 2A). No patient achieved a complete metabolic response (SUVs of all lesions equivalent to background) and 10 (50%) patients achieved a partial metabolic response (ΔSUV% < −25%). Four patients experienced an increase of ΔSUV% ranging from +6% to +36% and 2 of these were assessed with progressive metabolic disease (+25% ≤ ΔSUV%). These changes of target lesions in SUV at 2 days of treatment were compared with those in tumor size (ΔCTsize%) at 1 month of treatment, which was quantified on CT images, and there was a strong correlation ($R^2 = 0.496$; $P = 0.0008$) as shown in Fig. 2B. There was also a moderate agreement ($\kappa = 0.566$) between metabolic responses at 2 days based on the EORTC recommendations and morphologic overall responses at 1 month according to RECIST 1.0 (Fig. 2C). Of 10 metabolic responders at 2 days, 8 patients were morphologic responders and 2 were with stable disease by RECIST 1.0 at 1 month. Of 7 patients with stable metabolic disease (−25% ≤ ΔSUV% < +25%) at 2 days, 5 patients were assessed with morphologically stable disease and 2 had progressive disease by RECIST 1.0 at 1 month. Median PFS of patients with partial metabolic response, stable metabolic disease, and progressive metabolic disease was 290, 48, and 39 days, respectively. Median PFS of patients with morphologic partial response, stable disease, and progressive disease was 267, 100, and 29 days, respectively.

EGFR mutation

Biopsy samples from 5 patients were not suitable for molecular analysis. Mutation of *EGFR* gene was assessable in 15 patients and 12 were *EGFR* mutation positive: